Ore Geology Reviews 66 (2015) 403–421

Contents lists available at ScienceDirect

Ore Geology Reviews

journal homepage: www.elsevier.com/locate/oregeorev

Chalcophile elemental compositions and origin of the Tuwu porphyry Cu deposit, NW China

Jian-Feng Gao [a,b,*], Mei-Fu Zhou [b], Liang Qi [c], Wei Terry Chen [b], Xiao-Wen Huang [c]

[a] State Key Laboratory for Mineral Deposits Research, Nanjing University, Nanjing 210093, China
[b] Department of Earth Sciences, the University of Hong Kong, Hong Kong, China
[c] State Key Lab of Ore Deposit Geochemistry, Institute of Geochemistry, Chinese Academy of Sciences, Guiyang 550002, China

ARTICLE INFO

Article history:
Received 28 July 2014
Received in revised form 20 August 2014
Accepted 25 August 2014
Available online 29 August 2014

Keywords:
Platinum group elements (PGEs)
Porphyry Cu deposit
Re–Os isotope
Tuwu
NW China

ABSTRACT

The Tuwu porphyry Cu deposit in the eastern Tianshan Orogenic Belt of southern Central Oceanic Orogen Belt contains 557 Mt ores at an average grade of 0.58 wt.% Cu and 0.2 g/t Au, being the largest porphyry Cu deposit in NW China. The deposit is genetically related to dioritic and plagiogranitic porphyries that intruded the Carboniferous Qieshan Group. Ore minerals are dominantly chalcopyrite, pyrite and enargite. Porphyric diorites have Sr/Y and La/Yb_N ratios lower but Y and Yb contents higher than plagiogranites. Diorites have highly variable Cu but nearly constant PGE contents (most Pd = 0.50–1.98 ppb) with Cu/Pd ratios ranging from 10,900 to 8,900,000. Plagiogranites have PGEs that are positively correlated with Cu and have nearly uniform Cu/Pd ratios (5,100,000 to 7,800,000). Diorites have concentrations of Re (0.73–15.18 ppb), and $^{187}Re/^{188}Os$ and $^{187}Os/^{188}Os$ ratios lower but common Os contents (0.006–0.097 ppb) higher than plagiogranites. However, both the diorites and plagiogranites have similar normalized patterns of rare earth elements (REE), trace element and platinum-group elements (PGEs). All the samples are characterized by the enrichments of LREE relative to HREE and display positive anomalies of Pb and Sr but negative anomalies of Nb and Ta in primitive-mantle normalized patterns. In the primitive mantle-normalized siderophile element diagrams, they are similarly depleted in all PGEs but slightly enriched in Au relative to Cu.

Our new dataset suggests that both the diorite and plagiogranite porphyries were likely evolved from magmas derived from partial melting of a wet mantle wedge. Their parental magmas may have had different water contents and redox states, possibly due to different retaining time in staging magma chambers at the depth, and thus different histories of magma differentiation. Parental magmas of the diorite porphyries are relatively reduced with less water contents so that they have experienced sulfide saturation before fractional crystallization of silicate minerals, whereas the relatively more oxidized parental magmas with higher water contents of the plagiogranite porphyries did not reach sulfide saturation until the magmatic-hydrothermal stage. Our PGE data also indicates that the Cu mineralization in the Tuwu deposit involved an early stage with the enrichments of Au, Mo and Re and a late stage with the enrichment of As but depletion of Au–Mo. After the formation of the Cu mineralization, meteoric water heated by magmas penetrated into and interacted with porphyritic rocks at Tuwu, which was responsible for leaching Re from hosting rocks.

1. Introduction

Porphyry Cu deposits are important sources of copper metals in the world (Cooke et al., 2005; Sillitoe, 1997; Sillitoe, 2010; Ulrich et al., 1999). Most porphyry Cu deposits were produced in magmatic arcs above subduction zones of convergent plate margins (Sillitoe, 2010; Sun et al., 2013) and are thought to be closely linked to oxidized adakitic magmas (Ballard et al., 2002; Oyarzun et al., 2001; Sajona and Maury, 1998; Sun et al., 2010, 2013). Porphyry Cu deposits formed from reduced magmas are also known in literature (Cao et al., 2014a,b; Rowins, 2000; Smith et al., 2012; Sun et al., 2013). It appears that oxidized affinity of magmas is not a prerequisite for Cu mineralization in porphyry system but is important for the understanding of the origin of these deposits.

Porphyry Cu mineralization systems commonly involved both magmatic and hydrothermal processes. In the magmatic stage, distribution of platinum-group elements (PGEs) and Cu is controlled by the partition coefficients between sulfide and silicate melt, silicate mineral and other non-sulfide phases (Barnes and Maier, 1999; Fleet et al., 1991, 1999; Naldrett, 2004; Sattari et al., 2002). In the hydrothermal stage, PGEs would be preferably enriched in hot oxidized brines as chloride, hydroxide and sulfate complexes (Azaroual et al., 2001; Gammons, 1995, 1996; Gammons and Bloom, 1993; Gammons et al., 1992; Hanley, 2005;

* Corresponding author at: State Key Laboratory for Mineral Deposits Research, Nanjing University, Nanjing 210093, China.
E-mail address: gao_jianfeng@yahoo.com (J.-F. Gao).

http://dx.doi.org/10.1016/j.oregeorev.2014.08.009
0169-1368/

Mountain and Wood, 1988; Sassani and Shock, 1998; Wang et al., 2014) or in reduced sulfur-rich fluids as bisulfide complexes (Barnes and Liu, 2012; Gammons and Bloom, 1993; Mountain and Wood, 1988; Pan and Wood, 1994; Wood et al., 1994). However, Cu in magmatic-hydrothermal systems can be transported as hydrated copper-chloride or chloride complexes (Archibald et al., 2002; Hack and Mavrogenes, 2006; Liu and McPhail, 2005), which are sensitive to temperature, pressure, pH values and NaCl contents but not oxidization state. Therefore, due to their different behaviors, PGEs and Cu geochemistry in magmatic-hydrothermal systems can provide physiochemical information for the evolution of a porphyry mineralization system.

Currently, precise PGE data for porphyry Cu deposits are rarely reported possibly due to very low PGE concentrations of porphyritic rocks. Tarkian and Stribrny (1999) firstly reported the PGE data of different porphyry Cu deposits and found that PGE contents of porphyry Cu deposits are highly variable. Economou-Eliopoulos and Eliopoulos (2000) obtained Pd and Pt contents of porphyry Cu deposits in Greece and concluded that the oxidization state may be important for PGE enrichment. It was also indicated that PGEs of the Fengshan porphyry-skarn Cu–Mo deposit, eastern China, could be transported as various complexes in hydrothermal fluids under different temperatures (Wang et al., 2014). However, the linkage of redox condition with the transportation of PGE–Au–Cu in hydrothermal fluids is still poorly constrained and the relationship between magma differentiation and Cu mineralization needs more rigorous examination.

There are many giant porphyry Cu–(Mo) deposits in the Central Asian Orogenic Belt (CAOB) (Shen et al., 2014b). Among them, the Tuwu porphyry copper deposit is the largest one and is hosted in both dioritic and plagiogranitic porphyries. The Cu mineralization was thought to be genetically related to a magmatic-hydrothermal system associated with the emplacement of the plagiogranitic porphyry and the pre-mineralization dioritic porphyry is thought to have a different origin (Han et al., 2006; Liu et al., 2003, 2009; Rui et al., 2002; Shen et al., 2014b; Zhang et al., 2004, 2006b). However, the mineralization-related plagiogranite porphyry emplaced only a short time after the intrusion of the diorite porphyry. Both the porphyries at Tuwu are Cu-mineralized and ideal to use PGEs to investigate the redox states of the magmatic-hydrothermal system.

In this paper, we firstly report the Re–Os isotopic compositions of porphyry rocks as well as a new high quality dataset of whole rock geochemistry, particularly PGE and Au concentrations. Our objectives are to better understand the behaviors of PGEs and Cu in the porphyry Cu mineralizing system and to constrain the origin of the deposit and Re–Os isotopes in the porphyry system. We also demonstrate that both the dioritic and plagiogranitic porphyries have undergone different evolution in the magma-hydrothermal system. Our study further confirms that combining PGE elemental and Re–Os isotopic compositions can be a powerful tool to examine the origin of porphyry Cu deposits.

2. Geological background

2.1. Regional geology

Being one of the largest accretionary orogenic belts in the world, the CAOB is bounded by the Tarim Craton and North China Craton to the south, by the Siberian Craton to the north (Fig. 1a). The Tianshan Orogenic Belt is the southernmost part of the CAOB and extends for ca. 2500 km from Xinjiang, China to Kyrgyzstan and Kazakhstan (Fig. 1b) (Coleman, 1989; Gao et al., 1998; Windley et al., 1990).

The eastern Tianshan Orogenic Belt is composed of the Karlik Belt, Jueluotag Belt and Middle Tianshan Terrane from the north to the south, which are separated by the Kanggurtag–Huangshan, and Shaquanzi faults, respectively (Fig. 1c). These geological units have different rock associations and host distinct mineralization. The Karlik Belt comprises Ordovician–Carboniferous volcanic rocks, felsic and mafic–ultramafic intrusions. This belt contains only few porphyry Cu and Au prospects (Fig. 1c). The Jueluotag Belt is dominated by Middle Paleozoic volcanic and sedimentary rocks. There are numerous Carboniferous–Permian felsic and mafic–ultramafic intrusions along major regional faults in the Jueluotag Belt. The belt is composed of the Wutongwozi and Dananhu Arcs, Huangshan shear zone and Yamansu belt separated by the Kanggurtag–Huangshan and Yamansu faults (Fig. 1c). These three sub-belts have different geodynamic settings and rock types, associated with distinctive mineralization. Porphyry Cu–Au deposits in the Dananhu Arc occur along the Kanggurtag–Huangshan Fault (Zhang et al., 2006a). There are many magmatic Ni–Cu sulfide deposits associated with mafic–ultramafic intrusions in the Yamansu Belt (Gao and Zhou, 2013; Gao et al., 2013; Zhou et al., 2004). Various types of magnetite deposits are located in the southern part of the Yamansu Belt. Gold deposits are generally distributed along the faults that separated these sub-belts (Zhang et al., 2008). The Middle Tianshan Terrane has a Precambrian basement, and hosts some hydrothermal magnetite deposits (Fig. 1c).

The Paleozoic Dananhu Arc is mainly composed of Devonian to Jurassic sedimentary rocks and Cenozoic covers (Fig. 2a). The Lower Devonian Dananhu Formation only exposed to the north of the Dacaotan Fault mainly consists of mafic to intermediate-acid volcanic rocks and clastic sedimentary rocks. The Lower Carboniferous Gandun Formation is dominantly composed of turbidites with minor limestone and volcanic rocks, whereas the Lower-Middle Carboniferous Qieshan Group is made up of basalt, andesite, spilite, keratophyre, andesitic brecciated lavas, lithic sandstone, pebbly lithic sandstone, and conglomerate. The Permian Aqikebulake and Darequanzi Formations are dominantly of calc-alkaline volcanic, pyroclastic and clastic rocks. The Jurassic Xishanyao Formation consists of terrestrial clastic rocks of gray sandstones and mudstones interlayered with coal seams. Permian and older strata in the region have experienced ductile deformation and lower greenschist to prehnite–pumpellyite facies metamorphism.

In the Dananhu Arc, E–W trending faults include the Dacaotan and Kanggurtag faults. NW and NE trending faults are also presented in the region (Shen et al., 2014b). Paleozoic felsic and mafic rocks with ages ranging from 360 Ma to 252 Ma, including quartz diorites, plagiogranites, diorite porphyry, monzogranites and granites, are widespread in the Dananhu Arc (Shen et al., 2014a,b; Song et al., 2002; Zhang et al., 2010, 2014; Zhou et al., 2010). Porphyry Cu deposits spatially related to plagiogranite porphyries include the Yandong, Tuwu, Linglong and Chihu porphyry Cu deposits and form a metallogenic belt in the southern margin of the Dananhu Arc (Fig. 2a).

2.2. Geology of the Tuwu deposit

The Tuwu porphyry copper deposit is located about 2–5 km north of the Kanggurtag Fault. The deposit contains 557 Mt ores at an average grade of 0.58 wt.% Cu and 0.2 g/t Au (Liu et al., 2003; Rui et al., 2001), being the largest porphyry Cu deposit in NW China. Ore bodies are mainly hosted in plagiogranite and diorite porphyries (Fig. 2b) that intruded intermediate to mafic volcanic rocks of the Carboniferous Qieshan Group (Han et al., 2006; Liu et al., 2003; Zhang et al., 2004).

The Qieshan Group is composed of andesite and tuff (Unit 1), andesitic or basaltic breccia (Unit 2), sandstone and tuff with minor basalt–andesite (Unit 3), sandstone and siltstone with tuff and basalt interlayers (Unit 4), and gray to green conglomerate (Unit 5) from base upwards (Han et al., 2006; Shen et al., 2014b; Zhang et al., 2004, 2006b). Andesite of Unit 1 contains zircons with a SHRIMP U–Pb age of 336.5 ± 6.6 Ma (Hou et al., 2005).

2.2.1. Porphyries

Cu mineralization of the Tuwu deposit is hosted in both diorite and plagiogranite porphyries (Fig. 2b). The diorite porphyry body strikes roughly E–W and occupies a surface area of ~0.19 km^2 (Zhang et al., 2006b). Rocks have porphyritic texture with phenocrysts of plagioclase and biotite and the matrix of plagioclase, biotite, hornblende and quartz.

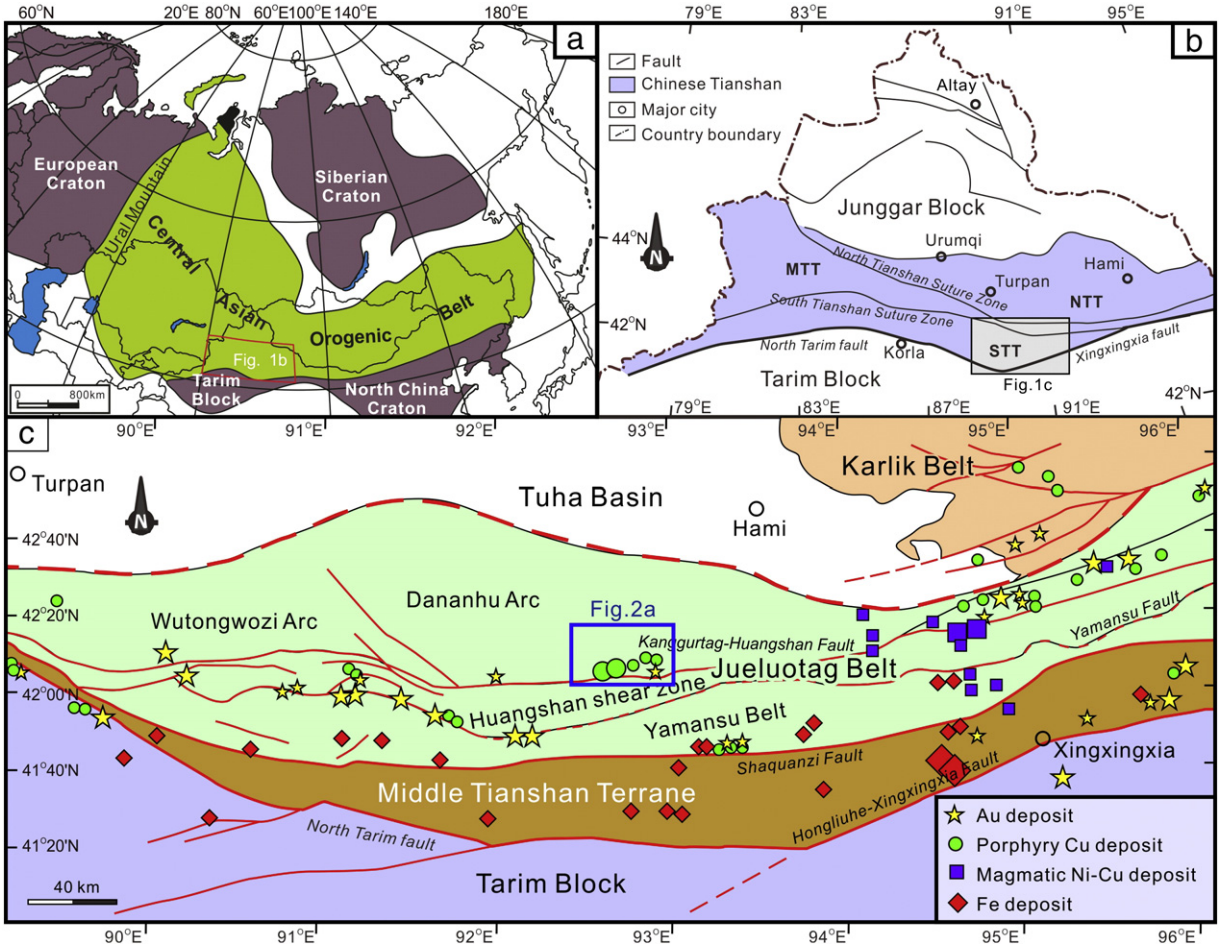

Fig. 1. Simplified geological maps showing a) the location of the CAOB; b) the Tianshan Orogenic Belt; and c) tectonic units of the eastern Tianshan Orogenic Belt.

There are 23 intrusive stocks and plugs of plagiogranite porphyries, the largest of which has a surface outcrop of ~0.03 km^2 (Han et al., 2006; Zhang et al., 2006b). Plagiogranite porphyries intruded the diorite porphyry and the Qieshan Group and occur as dykes. The rocks have porphyritic texture with phenocrysts of quartz, plagioclase and biotite and matrix of plagioclase, quartz, and biotite.

Both diorite and plagiogranite porphyries have undergone extensive hydrothermal alteration of silicification, sericitization, carbonatization, chloritization and kaolinitization (Han et al., 2006; Shen et al., 2014b; Zhang et al., 2004). The mineralized intrusions contain abundant quartz-sulfide and biotite–chlorite–sulfide veins (Fig. 3). The plagiogranite porphyry is thought to emplace at 332–334 Ma by SHRIMP or SIMS zircon U–Pb dating (Chen et al., 2005; Liu et al., 2003; Shen et al., 2014b). Precisely dating of the diorite porphyry is not available but the timing of its emplacement is possibly 333–336 Ma by the geological relationships with country rocks and the intruded plagiogranite porphyry.

2.2.2. Styles of mineralization

The Tuwu copper deposit consists of the Tuwu and Eastern Tuwu ore bodies (Fig. 2b), which are situated 200 m apart from each another. The Tuwu ore body is tabular or lentoid. It extends along an E–W direction, and has a maximum length of 1400 m and a thickness of up to 125 m at the surface. The ore body generally dips to the south and locally to the north. The copper grade of ores reaches 1.5% at the center of the Tuwu ore body, and gradually decreases from the center to the margin and then to hosting rocks. The Eastern Tuwu ore body has variable thicknesses (average 32 m, maximum 84 m), and dips steeply to the south. Ores in the thickest eastern part of the ore body have the highest ore grade (up to 1.5% Cu).

The Tuwu deposit comprises mainly disseminated and veinlet-like Cu ores. Ore minerals are dominantly chalcopyrite with variable amounts of pyrite and enargite (Fig. 3). There are also some minor bornite, chalcocite, digenite, sphalerite, malachite and rickardite. Gangue minerals are quartz, plagioclase, rutile, sericite, chlorite, biotite, epidote and calcite (Fig. 3). Locally, pyrite grains are replaced by magnetite and hematite. Chalcopyrite grains are commonly anhedral with grain sizes ranging from 0.05 to 1 mm, and they are generally closely associated with calcite and quartz (Figs. 3a–b; 4a–b), either in veins or in disseminated ores. Subhedral to anhedral pyrite grains (5 μm to 1 mm) are commonly present in quartz veins (Figs. 3b and 4d), whereas enargite is just locally present (Figs. 3c–f; 4e–f) as isolated grains are associated with quartz and chalcopyrite (Fig. 3c–d). Minor enargite grains are also enclosed in chalcopyrite or distributed along the margins of chalcopyrite grains in alteration zones (Figs. 3f; 4e–f). In addition, trace amounts of rutile (~30 μm) are also present, associated with chalcopyrite (Fig. 4a, c).

2.2.3. Paragenetic sequence of alteration and mineralization

There are six types of alteration in the Tuwu deposit, including the Ca–Na silicate, potassic, chlorite–sericite, phyllic, propylitic and argillic alterations. All six types of alterations occurred in the diorite porphyry, whereas only potassic, chlorite–sericite and phyllic alterations could be identified within plagiogranite porphyry (Shen et al., 2014b). The alterations associated with Cu mineralization include potassic, chlorite–sericite and phyllic alterations in both diorite and plagiogranite porphyries.

On the basis of the mineralogy and micro-textures, Cu mineralization of the Tuwu deposit can be divided into four stages: Stage I is

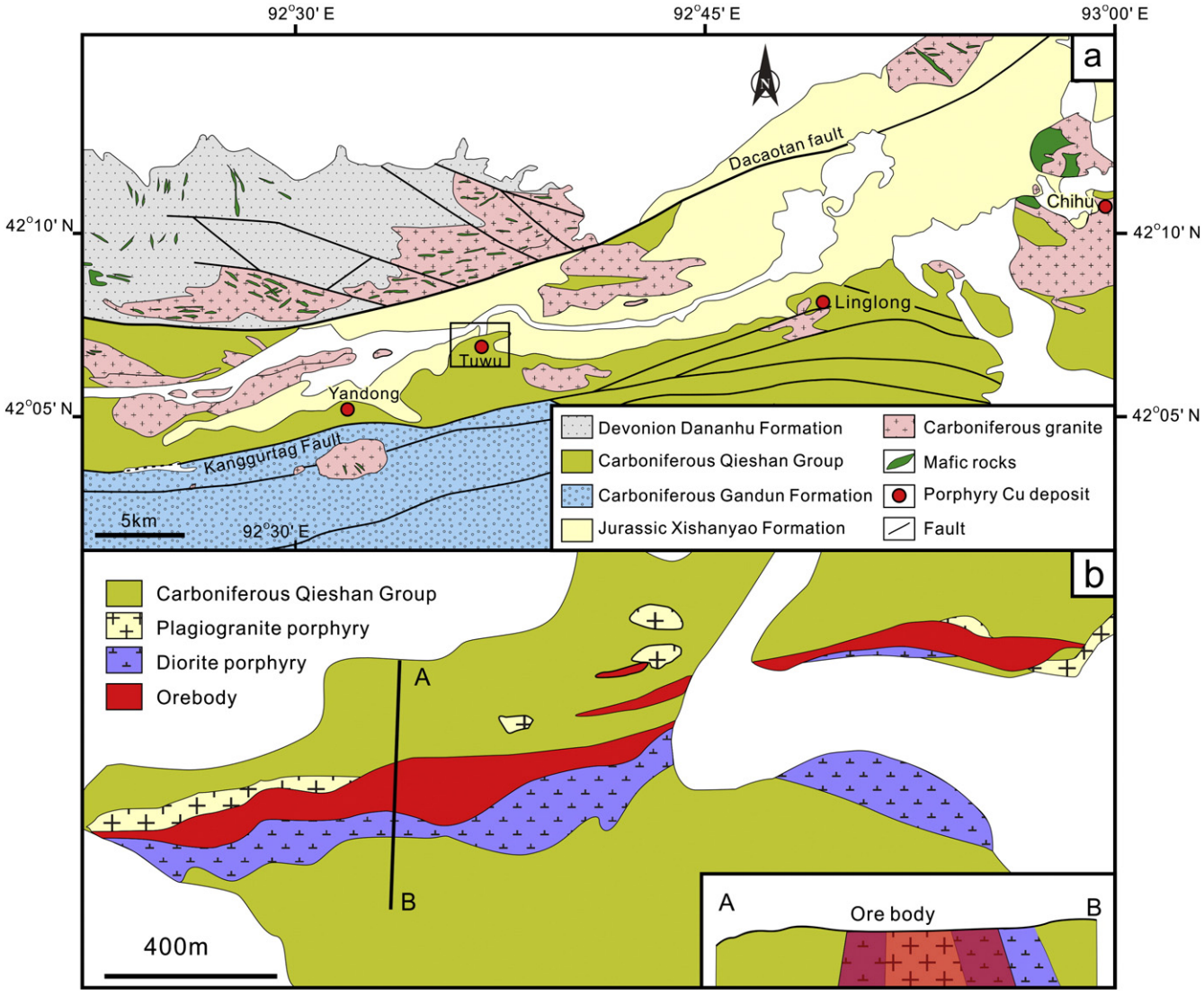

Fig. 2. a) Geological map of the Tuwu region showing the distribution of porphyry deposits; and b) Simplified geological map of the Tuwu porphyry Cu deposit.

characterized by vein-like and disseminated mineralization associated with potassic alteration with an assemblage of chalcopyrite + bornite + pyrite; Stage II is represented by extensive veins containing quartz + pyrite + chalcopyrite associated with chlorite–sericite–phyllic alteration; Stage III is characterized by an assemblage of quartz + molybdenite occurring as veins or disseminations in hosting rocks; and Stage IV consists of carbonates (calcite), laumontite and minor sulfides (Han et al., 2006; Shen et al., 2014b; Zhang et al., 2006b). Stage III and Stage IV are commonly associated with phyllic alteration.

3. Analytical methods

3.1. Whole rock major and trace elements

Major oxides and S were determined with a Philips PW2400 X-ray fluorescence (XRF) spectrometer on glass disks at the Department of Earth Sciences, HKU. The analytical precisions are better than 1% (RSD) for elements higher than 1 wt.% and 5% (RSD) for those lower than 1 wt.% and S.

Trace elements were measured with a PE DRC-e inductively coupled plasma mass spectrometry (ICP-MS) at the Institute of Geochemistry, Chinese Academy of Sciences, Guiyang, following the procedure described in Qi et al. (2000) and Gao et al. (2003). 50 mg of sample powder was precisely weighted and then decomposed by the mixture of 1 ml HF and 0.5 ml HNO_3 in the custom-made high-pressure Teflon bomb. Rh was added as internal standard to correct the signal drift of the instrument. Reference materials, GSR-1 (granite), BHVO-2 (basalt) and G-2 (granite), were used to monitor the trace element analyses. The precision for most trace elements is better than 5% (RSD) in terms of the results of reference standards.

3.2. Platinum-group elements, Au and Re–Os isotopes

PGE and Re concentrations and Re–Os isotopes were determined using isotope-dilution ICP-MS (ID-ICP-MS) in the Institute of Geochemistry, Guiyang, Chinese Academy of Sciences, with a revised Carius tube technique (Qi et al., 2007, 2010). ~8 g of sample powders was precisely weighted and transfered to Carius tube. Appropriate amounts of enriched isotope spike solutions of ^{105}Pd, ^{101}Ru, ^{185}Re, ^{190}Os, ^{193}Ir and ^{194}Pt were accurately weighted and added into samples combining with 15 ml of concentrated HCl and 20 ml of concentrated HNO_3. The sealed Carius tube was then placed in a stainless steel high-pressure autoclave that was sealed and heated to 330 °C in the oven for 12 h. After cooling, Os was collected by in situ distillation system and Re

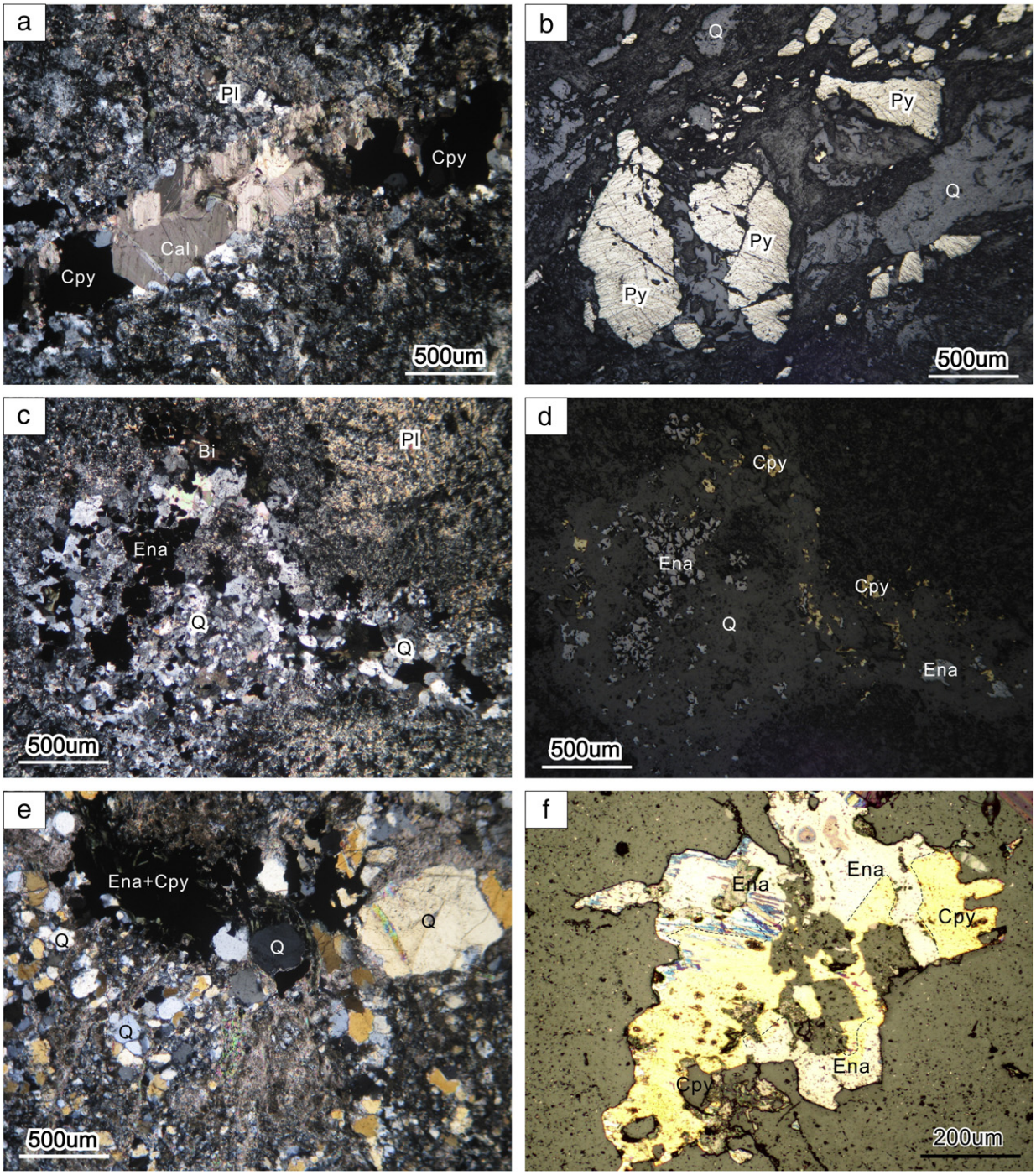

Fig. 3. Microphotographs of Tuwu porphyry rocks: (a) polarized transmitted light photograph of chalcopyrite–calcite vein in diorite porphyry (XTWG50); (b) reflected light photograph of pyrite–calcite–quartz vein in diorite porphyry (XTWG165); (c) transmitted and (d) reflected light photograph of disseminated chalcopyrite and enargite associated with quartz in diorite porphyry (XTWG43); (e) polarized transmitted and (f) reflected light photos of enargite and chalcopyrite in plagiogranite porphyry (XTWG55), enargite is closely associated with chalcopyrite. *Pl* — plagioclase, *Bi* — biotite, *Q* — quartz, *Cal* — calcite, *Py* — pyrite, *Cpy* — chalcopyrite, *Ena* — enargite.

was separated using Bio-rad AG 1-X8 anion exchange resin for Re–Os isotope analyses (Qi et al., 2010). Other PGEs in remaining solution were concentrated by Te-coprecipitation. The solution dissolved by Te-coprecipitation was passed through a mixed ion exchange resin of Dowex 50 W-X8 cation exchange and P507 extraction chromatograph resins to remove Cu, Ni, Zr, and Hf to minimize possible interference for PGE analyses (Qi et al., 2007). The sensitivity of the instrument was adjusted to more than 30,000 cps for 1 ng/ml In. Re, Os, Ir, Ru, Pd and Pt contents were measured with ID-ICP-MS and Rh was determined using ^{194}Pt as an internal standard (Qi et al., 2004). The analyses were monitored using standard reference materials, WPR-1 (peridotite), WGB-1 (gabbro) and TDB-1 (diabase). Procedural blanks of Re, Os, Ir, Ru, Rh, Pt and Pt are 20 pg, 2 pg, 25 pg, 20 pg, 30 pg, 0.2 ng and 0.40 ng, respectively. Analytical precision is estimated to be better than 15% from the replication of standard materials.

3.3. Sr–Nd isotopes

About 100 mg of powder was dissolved in Teflon beakers with a HF + HNO_3 mixture acid, and Sr and Nd were then separated and

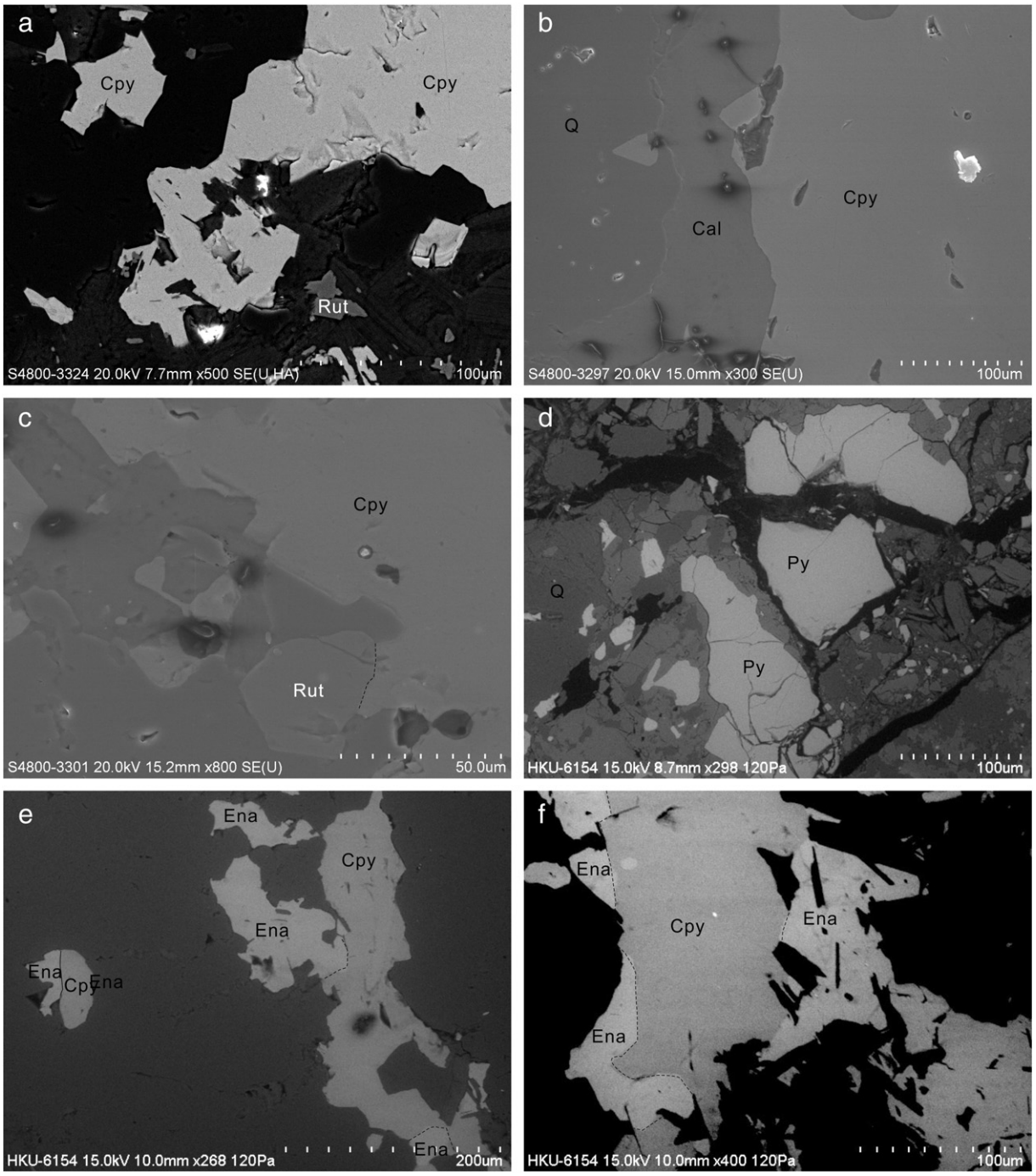

Fig. 4. Backscattered electron images of sulfides in Tuwu porphyries. (a) euhedral chalcopyrite grains in quartz–calcite vein in diorite porphyry (XTWG24), rutile is associated with Cu mineralization in the vein; (b) SEM image showing the boundary of quartz, calcite and chalcopyrite, chalcopyrite occurs as individual grains associated with calcite or inclusions in quartz; (c) The association of chalcopyrite and rutile in quartz vein in plagiogranite (XTWG55); (d) SEM image displaying the distribution of subhedral–anhedral pyrite grains in quartz–calcite vein (XTWG68); (e–f) SEM image illustrating the texture of the association of enargite and chalcopyrite. Enargite has clear boundaries with chalcopyrite. It occurs at the margin of chalcopyrite or inclusions in chalcopyrite, suggesting a later growth of enargite. *Q* — quartz, *Cal* — calcite, *Py* — pyrite, *Cpy* — chalcopyrite, *Ena* — enargite, *Rut* — rutile.

purified by adopting AG50Wx8 resin and different eluent reagents (DCTA and HIBA respectively) (Pu et al., 2005). The isotopic compositions of purified Sr and Nd solutions were measured using a Thermo Finnigan Triton TI thermal ionization mass spectrometer (TIMS) at the State Key Laboratory for Mineral Deposits Research, Nanjing University. $^{87}Sr/^{86}Sr$ and $^{143}Nd/^{144}Nd$ ratios are reported as measured, and normalized to $^{86}Sr/^{88}Sr$ of 0.1194 and $^{146}Nd/^{144}Nd$ of 0.7219, respectively. During the period of analysis, analyses of the La Jolla standard yielded an average value of $^{143}Nd/^{144}Nd = 0.511842 \pm 4$ (2σ, n = 5), and the NBS-987 Sr standard gave a mean value of $^{87}Sr/^{86}Sr = 0.710260 \pm 10$ (2σ, n = 5). Total procedure blanks were 50 pg for Nd and 200 pg for Sr, respectively.

4. Analytical results

All samples were collected from the surface outcrop of the diorite porphyry and drill hole ZK08 that penetrated the both plagiogranite and diorite porphyries of the Tuwu ore body. All samples are from the Tuwu ore body of the deposit.

4.1. Whole rock major and trace elements

Whole rock major and trace elements of samples from porphyries of Tuwu are presented in Appendix 1.

Rocks from both diorite and plagiogranite porphyry have variable major element oxides, reflecting varying modal mineralogy. Diorite porphyries have low SiO_2 (53.5 to 62.3 wt.%) but high TiO_2 (0.82 to 1.43 wt.%), MgO (2.61 to 11.85 wt.%) and $Fe_2O_3^T$ (6.69–10.74 wt.%). Plagiogranite porphyries have high SiO_2 (65.4 to 80.3 wt.%), low TiO_2 (0.26 to 0.79 wt.%), MgO (0.52 to 2.09 wt.%) and $Fe_2O_3^T$ (2.11 to 4.49 wt.%). Both rocks have variable Al_2O_3 (10.01–19.09 wt.% and 5.87–13.89 wt.%, respectively), Na_2O (1.96–5.53 wt.% and 1.49–4.34 wt.%, respectively) and K_2O (0.02 to 3.88 wt.% and 0.37–1.81 wt.%, respectively), possibly indicating various degrees of alteration, in particular potassic alteration.

Diorite porphyries have chondrite-normalized rare earth elements (REE) patterns similar to plagiogranite porphyries. Diorite porphyries have chondrite-normalized REE pattern enriched in light REE (LREE) with relatively fractionated high REE (HREE) (La/Sm = 1.96–4.6) and (Gd/Yb = 1.45–3.08) (Fig. 5a). These rocks display highly variable Eu anomalies (Eu/Eu* = 0.64–1.47). Plagiogranite porphyries have lower REE concentration than diorite porphyries. They are enriched in LREE (La/Sm = 2.76–4.1), but show unfractionated HREE on chondrite-normalized patterns (Gd/Yb = 2.01–2.55) and positive Eu anomalies (Fig. 5b).

Both diorite and plagiogranite porphyries have variable abundances of trace elements and show nearly flat primitive-mantle normalized patterns, with exceptions of enrichment of Pb and Sr and depletion of Nb and Ta (Fig. 5c–d). Diorite porphyries have highly variable large ion lithophile elements (LILE, e.g. Rb, Ba and Sr) (Fig. 5c), whereas plagiogranite porphyries are enriched in Rb, Ba, Sr and Pb (Fig. 5d).

4.2. Chalcophile elements (PGEs, Au, Cu and Ni)

Whole rock platinum group elements, Au, Cu and Ni of both diorite and plagiogranite porphyries are presented in Table 1. Diorite porphyries at Tuwu generally contain less sulfides with lower and more variable Cu than plagiogranite porphyries. Both diorite and plagiogranite porphyries have trough-shaped, primitive mantle-normalized siderophile element patterns with slight enrichment of Au relative to Cu (Fig. 6). However, plagiogranite porphyries have lower Ni and consequently higher Cu/Ni ratios (150–740) than diorite porphyries (Cu/Ni = 0.17–137).

Although diorite porphyries have highly variable Cu, most of them have relatively uniform PGEs contents (most Pd = 0.50–1.98 ppb) with Cu/Pd ratios ranging from 10,900 to 8,900,000 (Figs. 6a; 7a–b). On the contrary, PGEs in plagiogranite porphyries are positively correlated to Cu with nearly uniform Cu/Pd ratios (5,100,000 to 7,800,000) (Fig. 7a–b). Au in both diorite and plagiogranite porphyries is positively correlated with Cu (Fig. 7c). There is a negative correlation between Au and As in diorite porphyries, but not in plagiogranite porphyries (Fig. 7d).

4.3. Whole rock Sr–Nd isotopes

Rb–Sr and Sm–Nd isotopic data are given in Table 2. Diorite porphyries have variable $^{87}Rb/^{86}Sr$ ratios (0.005–1.67), initial $^{87}Sr/^{86}Sr$ ratios (0.7016 to 0.7060) and high εNd values (+4.1 to +7.5) (Fig. 8). The only plagiogranite porphyry sample analyzed has $^{87}Rb/^{86}Sr$ ratio of 0.21, initial $^{87}Sr/^{86}Sr$ ratio of 0.7035 and εNd value of, +7.5 (Table 2, Fig. 8). Most samples from the Tuwu deposit are plotted on the mantle array area between the depleted mantle and Carboniferous volcanic rocks from Tianshan (Xia et al., 2008) (Fig. 8).

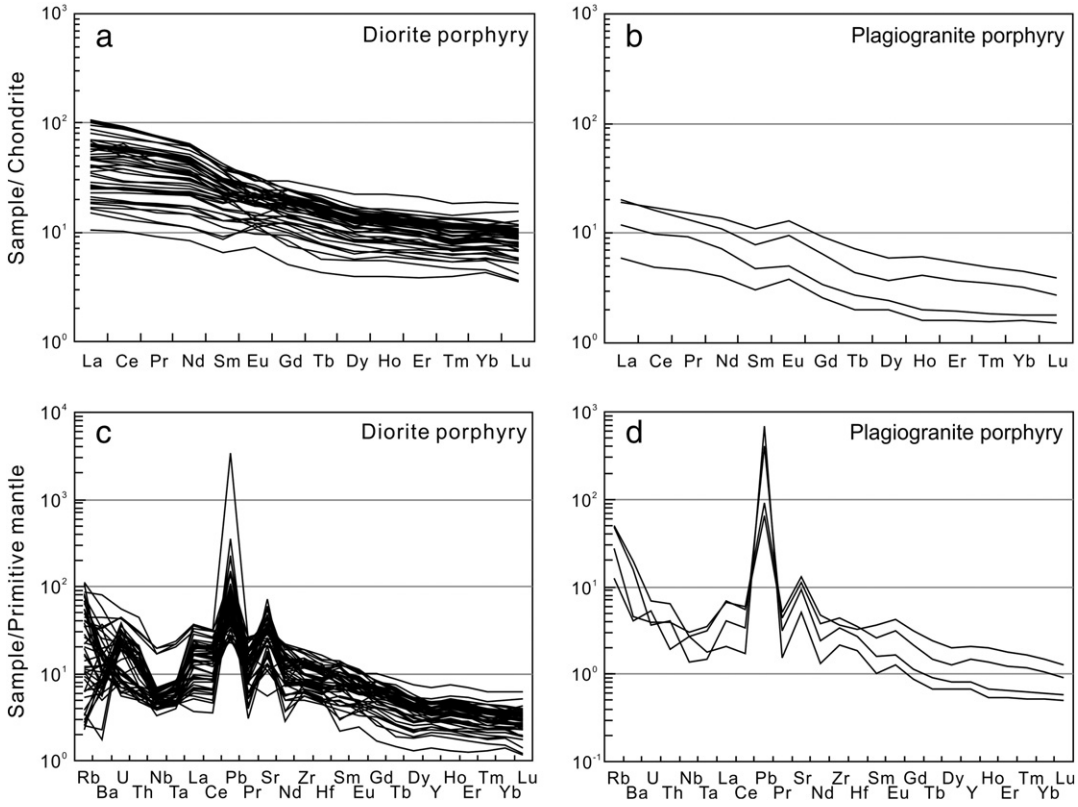

Fig. 5. Chondrite-normalized REE patterns of porphyry rocks (a — diorite porphyry; b — plagiogranite porphyry); Primitive-mantle normalized trace element patterns of (c) diorite porphyry, and (d) plagiogranite porphyry. Normalization values are from Sun and McDonough (1989).

Table 1
Contents of siderophile elements in the porphyries from the Tuwu deposit.

Sample	TWG901	TWG902	TWG903	TWG904	TWG905	TWG907	TWG908	TWG909	TWG910	TWG911	TWG912	TWG913	TWG914	TWG915	TWG916	XTWG15	XTWG16
Lithology	Diorite porphyry																
Co	22.4	16.7	21.8	27.9	20.5	18.4	17.4	19.6	16.4	18.6	21.2	20.0	21.2	26.4	29.7	22.3	26.6
Ni	84	89	63	62	59	48	161	90	73	57	50	58	51	51	47	58	115
Cu	342	294	269	261	434	604	445	229	171	421	400	843	14.1	8.6	46.0	3840	1030
Ir	0.012	0.011	0.010	0.009	0.008	0.011	0.011	0.012	0.010	0.014	0.011	0.014	0.010	0.008	0.008	0.022	0.023
Ru	0.023	0.021	0.036	0.023	0.027	0.020	0.034	0.026	0.024	0.019	0.029	0.026	0.033	0.031	0.023	0.026	0.053
Rh	0.018	0.022	0.067	0.032	0.041	0.027	0.049	0.016	0.017	0.054	0.033	0.033	0.012	0.010	0.029	0.045	0.053
Pt	1.22	0.44	0.51	0.55	0.33	0.58	0.49	0.44	0.56	0.76	0.82	0.97	0.59	0.53	0.91	0.44	0.46
Pd	1.01	0.78	0.77	0.75	0.96	0.65	0.74	0.85	1.00	0.90	1.07	0.81	0.75	0.79	1.11	1.24	0.70
Au	1.01	15.7	0.61	22.3	5.6	12.5	2.8	3.2	6.4	8.2	15.3	13.0	1.6	1.7	7.0	83	57

Table 1 *(continued)*

Sample	XTWG22	XTWG24	XTWG27	XTWG30	XTWG34	XTWG36	XTWG43	XTWG44	XTWG45	XTWG50	XTWG66	XTWG68	XTWG18	XTWG84	XTWG88	XTWG92	XTWG94
Lithology	Diorite porphyry																
Co	15.2	20.2	20.4	18.3	18.5	16.5	18.6	14.0	20.8	15.3	31.2	25.5	37	26.5	34	32	39
Ni	67	103	75	72	71	58	77	55	61	58	79	81	85	137	121	137	141
Cu	5120	3290	2620	1290	1290	2308	3660	6290	8300	5920	685	888	536	287	576	109	84
Ir	0.022	0.058	0.022	0.017	0.025	0.032	0.011	0.009	0.012	0.011	0.013	0.011	0.020	0.046	0.019	0.031	0.040
Ru	0.034	0.030	0.018	0.026	0.039	0.030	0.026	0.075	0.040	0.027	0.028	0.023	0.067	0.080	0.051	0.067	0.061
Rh	0.058	0.167	0.067	0.050	0.016	0.051	0.038	0.029	0.029	0.035	0.077	0.013	0.093	0.037	0.027	0.021	0.029
Pt	0.45	0.71	0.33	0.42	0.38	0.53	0.49	0.39	0.73	0.29	0.28	0.20	0.22	0.63	0.88	0.57	1.12
Pd	1.14	1.01	1.07	0.71	0.67	1.17	1.17	1.08	1.11	0.67	1.19	0.50	21.5	0.65	1.16	0.76	1.26
Au	72	310	200	226	87	162	141	290	323	321	18.2	16.3	10.0	68	31	44	28.7

Table 1 (*continued*)

Sample	XTWG100	XTWG152	XTWG156	XTWG159	XTWG164	XTWG165	XTWG178	XTWG179	XTWG184	XTWG186	XTWG189	XTWG196	XTWG198	XTWG201	XTWG19	XTWG40	XTWG53	XTWG55
Lithology	Diorite porphyry														Plagiogranite porphyry			
Co	35	26.7	36	40	46	33	32	37	29.1	18.2	38	29.1	27.9	34	10.3	6.4	6.0	8.5
Ni	128	155	112	113	138	107	115	128	97	5.3	131	75	68	124	49	12.3	29.1	12.6
Cu	140	109	658	407	1591	336	316	1196	243	22	98	1134	848	91	7370	3150	11956	9319
Ir	0.032	0.055	0.037	0.040	0.039	0.026	0.035	0.033	0.029	0.003	0.037	0.019	0.016	0.031	0.020	0.012	0.007	0.009
Ru	0.058	0.140	0.105	0.124	0.090	0.046	0.104	0.078	0.056	0.034	0.047	0.020	0.031	0.061	0.109	0.023	0.054	0.057
Rh	0.023	0.030	0.064	0.062	0.054	0.024	0.047	0.169	0.028	0.004	0.027	0.035	0.053	0.023	0.023	0.069	0.024	0.016
Pt	0.91	1.03	0.60	0.71	0.74	0.60	0.63	0.66	0.59	0.01	0.77	0.48	0.45	0.90	0.49	0.006	1.49	0.31
Pd	0.83	0.98	1.20	0.92	0.88	0.92	0.82	1.98	0.81	0.21	0.92	1.00	0.63	1.04	1.38	0.51	2.35	1.20
Au	11.6	73	74	10.3	32	7.7	23.5	19.3	11.7	8.1	39	54	21.9	4.5	77	136	1590	120

4.4. Whole rock Re–Os isotopes

Fifteen diorite porphyry samples and two plagiogranite porphyry samples from the Tuwu deposit were analyzed for Re–Os isotopic compositions (Table 3; Fig. 9).

Diorite porphyries have 0.73 to 15.2 ppb Re and 0.006 to 0.097 ppb common Os, with $^{187}Re/^{188}Os$ ratios of 8.65 to 6530 and $^{187}Os/^{188}Os$ ratios of 0.187 to 25.7. Plagiogranite porphyries have relatively high Re (45.1 to 90 ppb) and low common Os (0.0039 to 0.0072 ppb), with high $^{187}Re/^{188}Os$ (56,400 to 59,800) and $^{187}Os/^{188}Os$ ratios (178 to 194) (Fig. 9a).

Most diorite and plagiogranite porphyry samples have high Re but low common Os and are identical to "LLHR" (Low-level, highly radiogenic) samples as defined by Stein et al. (2000). Therefore, the Re–Os model ages of these samples can be calculated by ^{187}Re and ^{187}Os contents. LLHR diorite porphyry samples ($^{187}Re/^{188}Os$ ratios > 2000) have model ages from 210 to 236 Ma with a weighted average of 223 ± 14 Ma (MSWD = 0.84); whereas plagiogranite porphyry samples have model ages from 189 to 195 Ma with a weighted average of 192 ± 22 Ma (MSWD = 0.055). Diorite porphyries with low $^{187}Re/^{188}Os$ ratios (<2000) have older model ages from 252 Ma to 1395 Ma due to different amounts of common Os. Isochron plots of $^{187}Re/^{188}Os$ versus $^{187}Os/^{188}Os$ ratios are used and uncertainty correlation factors are also included in the regression analysis. Regression of all samples from diorite and plagiogranite porphyries yields a model 1 isochron age of 218 ± 13 Ma (1σ, MSWD = 18; Fig. 9a), with an initial $^{187}Os/^{188}Os$ ratio of 0.34 ± 0.26. Regression of diorite porphyry samples with $^{187}Re/^{188}Os$ ratios <2000 yields an older model 1 isochron age of 259 ± 40 Ma (1σ, MSWD = 19; Fig. 9a), with a lower initial $^{187}Os/^{188}Os$ ratio of 0.21 ± 0.16.

Common Os in porphyry rocks are roughly negatively correlated to Re, resulting in different correlations with Re–Os model ages. Samples with young model ages have relatively low common Os concentrations and there is no correlation between common Os concentrations and model ages, whereas samples with young model ages are rich in Re and display an enrichment trend with decreasing model ages (Fig. 9b).

5. Discussion

5.1. Evaluation of analytical method for PGEs in porphyries

In previous studies, lead fire assay (Economou-Eliopoulos and Eliopoulos, 2000) and nickel sulfide (NiS) fire assay (Eliopoulos and Economou-Eliopoulos, 1991; Tarkian and Stribrny, 1999; Wang et al., 2014) were commonly used for the determination of PGEs and Au in porphyry rocks.

In lead fire assay procedures, PGEs and Au are separated from sample matrix by reductive fusion (sodium carbonate, borax, litharge and flour or charcoal) and collected in lead button. The detection limits of this technique are reported as 2, 0.1, and 0.5 ng/g for Au, Pt and Pd, respectively (Hall and Pelchat, 1994) (Table 4). NiS fire assay is more powerful and convenient in collecting chalcophile elements in geological samples (Asif and Parry, 1991; Gros et al., 2002; Hall and Pelchat, 1994; Hoffman et al., 1978; Jackson et al., 1990; Juvonen et al., 2002; Oguri et al., 1999; Ravizza and Pyle, 1997; Sun and Sun, 2005; Sun et al., 1998) (Table 4). Different from the lead fire assay technique with variable flux compositions for different samples, same fusion (5 g Ni powder, 3 g S, 20 g sodium tetraborate, 10 g sodium carbonate and 5 g quartz) is used for NiS FA. PGEs and Au are enriched in the nickel button. Detection limits (0.01 to 0.39 ng/g for Rh and Ir, respectively) are much lower than those of lead fire assay because most agents can be purified (Sun et al., 1998) (Table 4). Ravizza and Pyle (1997) applied the ID technique in nickel fire assay, which allows precise determination PGE even under low recoveries. However, most porphyry rocks have low concentrations of PGE and Au (low- to sub-ppb level) so that fire

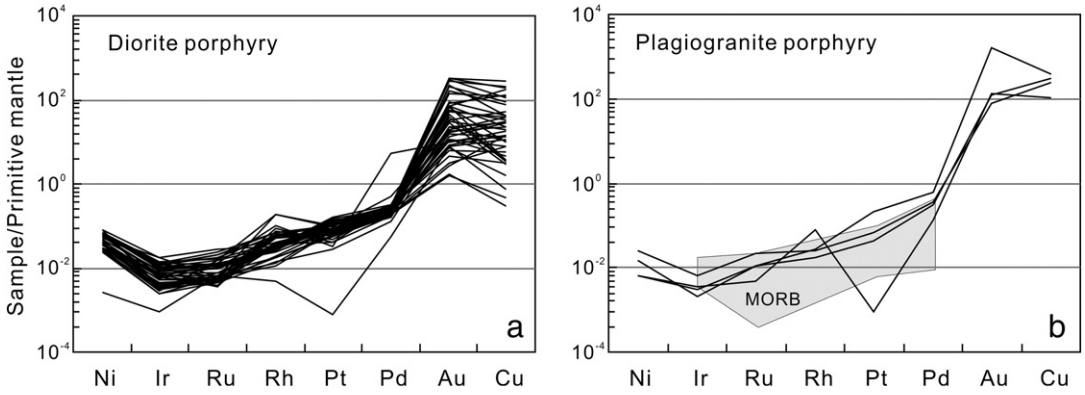

Fig. 6. Primitive-mantle-normalized chalcophile element patterns of silicate rocks and sulfide ores. PGE are represented in whole rock compositions. PGE contents of glasses in MORB are from Sun and McDonough (1989); (Bézos et al., 2005). Normalization values are from McDonough and Sun (1995); Barnes and Maier (1999); Barnes and Lightfoot (2005).

assay techniques might not be possible to accurately determine PGE and Au in these samples.

Acid digestion technique is extensively used for the determination of PGEs and Au in geological samples due to easy purification (Barefoot and Van Loon, 1999; Gowing and Potts, 1991; Li et al., 2014; Qi et al., 2010, 2011, 2013; Savard et al., 2010). In this technique, 0.5–5 g of sample powders is decomposed by mixtures of HCl and HNO_3 and/or HF. In order to enhance the recovery in acid digestion techniques, close digestion techniques, such as autoclave (Torgov et al., 1996), microwave (Totland et al., 1995), high pressure bomb Qi et al. (2011), HPA-S (high pressure asher, Anton Paar) (Meisel and Moser, 2004; Meisel et al., 2001, 2003; Moser et al., 2003; Pearson and Woodland, 2000) and Carius tube digestion techniques (Hassler et al., 2000; Qi et al., 2007, 2010, 2013; Rehkämper et al., 1998; Shirey and Walker, 1995) have been introduced for the determination of PGEs and Au in geological samples. The detection limits can be highly variable by using different techniques (Table 4).

The advantage and disadvantage of these digestion techniques discussed above are summarized in Table 5. In general, the fire assay allows a large amount of sample mass (up to 20 g) so that "nugget effect" of PGE can be minimized. However, fire assay techniques have relatively high procedure backgrounds. Among all techniques, acid digestion has provided the lowest procedure blanks and detection limits (Table 4). Revised Carius tubes can digest sample mass up to 12 g with

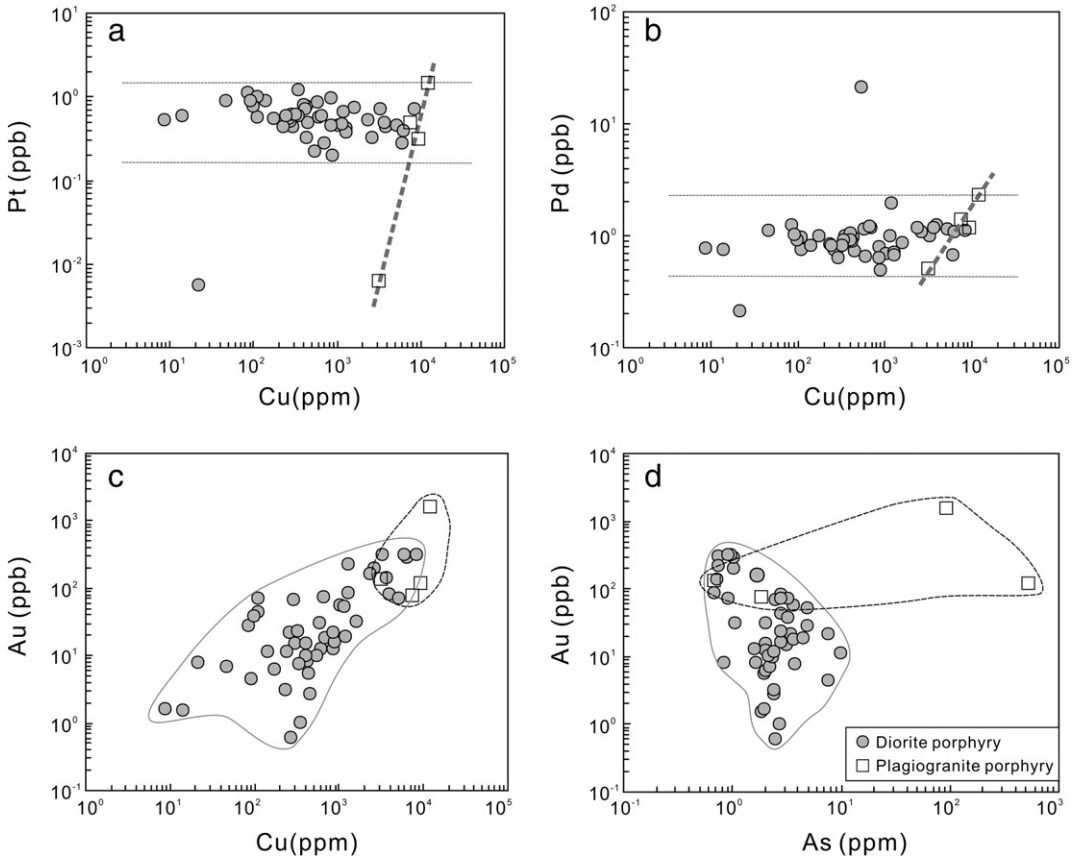

Fig. 7. (a) Plots of Cu vs Pt and (b) plots of Cu vs Pd of Tuwu porphyries showing different correlations between Cu and PGE in diorite and plagiogranite porphyries; (c) Plots of Cu vs Au illustrating positive correlation between these two elements in both porphyries at Tuwu; (d) plots of As vs Au showing negative correlations of As with Au in diorite porphyry and no correlation in plagiogranite porphyry.

Table 2
Sr–Nd isotopic compositions of diorite and plagiogranite porphyries of the Tuwu deposit.

	Lithology	Rb	Sr	$^{87}Rb/^{86}Sr$	$^{87}Sr/^{86}Sr$	2σ	$^{87}Sr/^{86}Sr_i$	Sm	Nd	$^{147}Sm/^{144}Nd$	$^{143}Nd/^{144}Nd$	2σ	$^{147}Nd/^{144}Nd$	εNd(t)
TWG902	DP	1.59	273	0.016	0.703730	3	0.7037	2.93	10.3	0.1793	0.512939	3	0.1510	6.6
TWG906	DP	6.0	248	0.068	0.706275	5	0.7060	6.5	25.1	0.1627	0.512918	2	0.1510	6.9
TWG915	DP	13.9	684	0.057	0.703814	11	0.7035	4.6	18.8	0.1526	0.512834	4	0.1510	5.7
XTWG16	DP	69	117	1.67	0.709420	4	0.7016	2.33	9.88	0.1486	0.512746	11	0.1510	4.1
XTWG44	DP	31	377	0.24	0.704449	4	0.7033	0.95	3.78	0.1589	0.512803	13	0.1510	4.8
XTWG66	DP	22.7	492	0.13	0.703963	9	0.7034	5.5	28.8	0.1197	0.512848	8	0.1510	7.3
XTWG88	DP	70	228	0.87	0.707130	3	0.7030	4.3	19.4	0.1400	0.512806	12	0.1510	5.7
XTWG100	DP	16.7	1240	0.038	0.703794	8	0.7036	2.72	9.8	0.1742	0.512972	4	0.1510	7.5
XTWG156	DP	2.12	1200	0.005	0.703657	3	0.7036	4.2	20.4	0.1307	0.512862	4	0.1510	7.2
XTWG186	DP	55	877	0.18	0.705924	7	0.7051	5.9	25.9	0.1426	0.512680	2	0.1510	3.1
XTWG196	DP	7.7	601	0.036	0.703840	8	0.7037	4.6	21.6	0.1351	0.512876	3	0.1510	7.2
XTWG53	PP	8.1	107	0.21	0.704540	7	0.7035	0.43	2.02	0.1329	0.512880	6	0.1510	7.4

Note: DP — diorite porphyry; PP — plagiogranite porphyry.

quantitative recoveries, which is efficient to minimize the "nugget effect". Thus, this technique is suitable in the determination of PGEs in low-PGE samples and is adopted in this study.

5.2. Magma sources of the porphyries

Diorites have relatively low Sr/Y and La/Yb ratios but high Y and Yb contents similar to the normal arc rocks (Fig. 10). Plagiogranites have Sr (107–223 ppm) and high Sr/Y (29–54) and La/Yb (5.6–9.7) ratios (Appendix 1; Fig. 10). Although these ratios are lower than typical adakites formed from magmas by melting of downgoing oceanic slab (e.g. Defant and Drummond, 1990; Kay, 1978; Martin et al., 2005), they have broadly adakitic affinities (Fig. 10) (Han et al., 2006; Shen et al., 2014b; Zhang et al., 2006b).

Adakite was thought to be generated by partial melting of subducting oceanic slabs (Defant and Drummond, 1990; Martin, 1999; Martin et al., 2005; Oyarzun et al., 2001; Sajona and Maury, 1998), or produced by partial melting of lower crust (Hou et al., 2004, 2009; Wang et al., 2006, 2007) or various mantle sources (Li et al., 2008; Macpherson et al., 2006; Richards, 2003, 2009; Zheng et al., 2012). The plagiogranites at Tuwu were previously considered to have derived from magmas by partial melting of subducted oceanic slabs (Han et al., 2006; Shen et al., 2014b; Zhang et al., 2006b). However, on the diagrams of Y vs Sr/Y and $Yb_{(n)}$ vs $La/Yb_{(n)}$ (Fig. 10), plagiogranite porphyry samples from this study and Zhang et al. (2006b) are not entirely plotted in the adakite field, and even some diorite samples display adakitic affinity (Fig. 10).

Adakitic affinity is commonly considered to be produced by partial melting at the depth where plagioclase becomes unstable to release Sr and garnet becomes stable to accommodate high REE (HREE) and Y (Moyen, 2009). Such a process would enhance Sr/Y and La/Yb ratios in magmas with increasing pressures. On the other hand, variable Sr/Y ratios in silicate magmas may be also contributed by different sources with different compositions (e.g. MORB with Sr/Y <5; continental crust with Sr/Y = 10–15; arc basalts with Sr/Y > 15) (Moyen, 2009). At a certain pressure, melts by partial melting of oceanic slab (MORB) would have relatively low Sr/Y ratios compared to melts derived from the continental crust or arc basalts. Plagiogranites have variable $_{Nd(t)}$ values (−1.4 to +9.3, mostly +5.0 to +9.3), indicative of involvement of continental crust materials, possibly having contributions on high Sr/Y and La/Yb ratios as well. Thus, the partial melting of subducting slab is not the only possibility to explain the adakitic affinity of plagiogranite porphyries. In addition, PGE contents of plagiogranite porphyries are comparable to that in Mid-Oceanic Ridge basalts (MORBs) (Fig. 6) (Bézos et al., 2005), we thus argue against an interpretation that the magma of plagiogranites was formed by partial melting of oceanic slab because such melting would generate silicate melts with PGE contents lower than the source rocks. In contrast, both diorite and plagiogranites have similar REE and trace element patterns (Fig. 5) and PGE patterns (Fig. 6). Thus, both diorite and plagiogranite porphyries are possibly derived from similar magmas in a mantle wedge but underwent different fractionation histories.

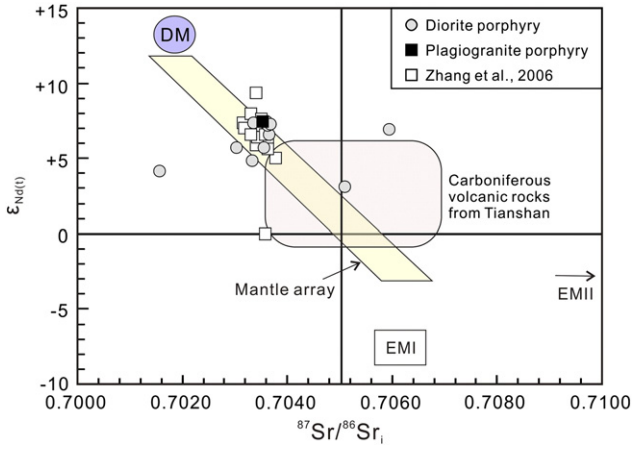

Fig. 8. Plot of ε_{Nd} (330 Ma) versus initial $^{87}Sr/^{86}Sr$ for the Tuwu porphyry. Reference fields are after Zindler and Hart (1986), ranges of Carboniferous volcanic rocks from Tianshan are from Xia et al. (2008).

5.3. Possible controls on magma differentiation

Fractionation of different minerals would have different controls on the La/Yb and Sr/Y ratios of magmas. Due to high partition coefficients for HREE in amphibole, fractionation of amphibole would decrease La/Yb ratios in evolved magmas (Davidson et al., 2007). Fractionation of amphibole is generally associated with that of plagioclase with high Sr/Y ratios, possibly resulting in increase of La/Yb ratios but moderately increase or even decrease of Sr/Y ratios of the residual magma. Adakitic signatures can also result from the removal of garnet at the depth because garnet is significantly enriched in HREE (Macpherson et al., 2006). Experimental studies have demonstrated that garnet can crystallize from calc-alkaline magmas at relatively high pressures (>12 kbar) (Alonso-Perez et al., 2009; Müntener and Ulmer, 2006; Müntener et al., 2001). Plagioclase is not stable under such high pressure so that garnet can crystallize individually or be garnet-dominant, significantly increasing the Sr/Y and La/Yb ratios in magmas.

Both diorites and plagiogranites have positive correlations between La/Yb ratios and La contents (Fig. 11a), indicating that fractional crystallization plays a dominant role on magma differentiation and thus may have produced high Sr/Y and La/Yb ratios of evolved magma. Plagiogranites exhibit steeper slope of correlation of Yb and La/Yb than diorites, corresponding to the fractionation of more garnet in magmas. Experiments indicate that magmas with more H_2O are able to crystallize more igneous garnet (Alonso-Perez et al., 2009). Thus, different magma

Table 3
Whole rock Re–Os isotopic compositions of diorite and plagiogranite porphyries of the Tuwu deposit.

	Lithology	Re (ppb)	1σ	Os (ppb)	1σ	$^{187}Re/^{188}Os$	1σ	$^{187}Os/^{188}Os$	1σ	Model age
XTWG-15	DP	3.4	0.2	0.0161	0.0015	1013	103	4.26	0.12	252
XTWG-27	DP	12.0	0.5	0.0124	0.0009	4652	384	18.3	0.4	235
XTWG-34	DP	8.6	0.1	0.0086	0.0003	4814	164	16.9	0.5	210
XTWG-36	DP	15.2	0.9	0.0131	0.0007	5617	437	22.4	0.6	239
XTWG-44	DP	5.2	0.3	0.0120	0.0004	2101	139	8.15	0.47	232
XTWG-45	DP	11.8	0.5	0.0087	0.0006	6535	528	25.70	0.41	236
XTWG-84	DP	0.077	0.004	0.043	0.004	8.65	1.0	0.204	0.012	1395
XTWG-88	DP	5.2	0.3	0.0173	0.0008	1460	101	6.75	0.22	277
XTWG-100	DP	0.174	0.011	0.0161	0.0015	52.5	5.7	0.685	0.019	779
XTWG-156	DP	0.54	0.04	0.042	0.001	61.7	4.3	0.388	0.012	377
XTWG-164	DP	0.297	0.010	0.097	0.017	14.7	2.7	0.203	0.009	819
XTWG-179	DP	0.33	0.03	0.032	0.003	50.5	6.3	0.264	0.005	313
XTWG-189	DP	0.073	0.006	0.0176	0.0007	19.9	1.7	0.187	0.008	560
XTWG-196	DP	0.44	0.02	0.0062	0.0005	340	28	1.61	0.07	284
XTWG-201	DP	0.224	0.021	0.0147	0.0008	73.4	7.8	0.875	0.029	711
XTWG-19	PP	90	6	0.0072	0.0002	59,826	4011	194	11	195
XTWG-53	PP	45	2	0.0039	0.0002	56,399	3838	178	6	189

Note: DP — diorite porphyry; PP — plagiogranite porphyry.

evolution processes for the plagiogranites and diorites are likely controlled by the water contents of magmas.

Richards (2011) also pointed out that differentiation of mantle-wedge derived arc magmas associated with increasing water contents can increase Sr/Y and La/Yb ratios in the evolved magmas. Magmas with large amounts of water (>4 wt.%) are able to fractionate amphibole ± garnet but suppression of plagioclase crystallization at a staging magma chamber at deep (e.g., the porphyry Cu deposits in Philippines) (Coldwell et al., 2011; Macpherson et al., 2006). We thus suggest that the plagiogranites at Tuwu was likely derived from magmas generated by partial melting of hydrous mantle wedge so that the parental magma can be water-rich and is able to fractionate amphibole and/or garnet. Different Y and Sr/Y ratios of the diorites and plagiogranites are likely ascribed to the different water contents of their parental magmas which have undergone variable amounts of amphibole ± garnet in the staging magma chambers.

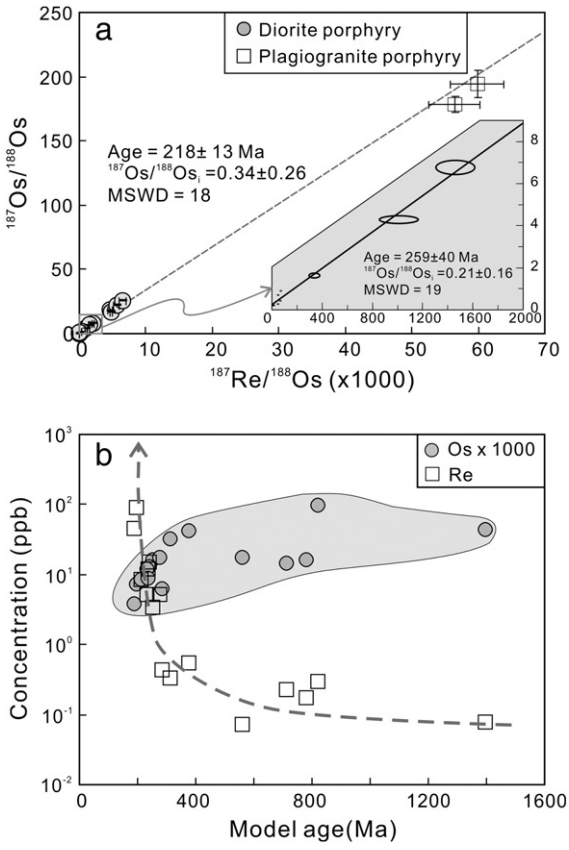

Fig. 9. (a) $^{187}Re/^{188}Os$ ratios vs $^{187}Os/^{188}Os$ ratios for Tuwu porphyries, zoomed diagrams in the right showing the isochron age of diorite porphyry with low $^{187}Re/^{188}Os$ ratios (<2000); (b) diagram of model ages vs Os and Re abundance showing that the model age is dominant by the enrichment of Re.

Arc magmas have highly variable water contents (1–8 wt.%) (Kelley and Cottrell, 2009; Nicholls and Ringwood, 1973; Schmidt and Poli, 1998; Sisson and Layne, 1993; Sobolev and Chaussidon, 1996). Primary arc magmas commonly contain only 1–3 wt.% of initial water (Sobolev and Chaussidon, 1996), and high initial water contents (6–8 wt.%) in arc magmas have been discovered in Mariana and Chile (Cooke et al., 2005; Kelley et al., 2010; Parman et al., 2011; RodrÍguez et al., 2007), which are related to subduction rate and temperature (van Keken et al., 2011), nature of subduction slab (Cooke et al., 2005; Parman et al., 2011; RodrÍguez et al., 2007), relative location of magmatism in the arc (Wallace, 2005), and remaining time in deep crustal chambers (Richards, 2011). Thus, most arc magmas would not contain high water contents. Water-rich magmas needed for magmatic-hydrothermal systems can only be generated under certain conditions.

The diorite porphyry emplaced about 1–2 Ma earlier than the plagiogranite porphyry at Tuwu (Chen et al., 2005; Han et al., 2006; Shen et al., 2014b; Zhang et al., 2006b). As such, the nature of subduction slab and subduction rate would not change a lot in such a short time. In addition, both the plagiogranites and diorites were formed from magmas derived from similar sources. Thus, only the differentiation of the magmas in deep crustal chambers would potentially produce different water contents of the magmas for the two types of rocks. Richards (2011) indicated that more remaining time for magmatic systems in deep crust could increase water contents so that more hydrous melts would form relatively late in a mature arc. Thus, high water and high sulfur magmas commonly emplaced after several million years of barren magmas (Chiaradia et al., 2009; Richards, 2003), a situation that is consistent with that at Tuwu.

In summary, parental magmas of the diorites and plagiogranite porphyries might have had different water contents, which were likely related to their different evolving time at the depth crust in staging magma chambers.

5.4. Redox states of magmas

Although the plagiogranite porphyry emplaced after the diorite porphyry in a short time (~2 Ma), the two types of rocks are different in terms of PGE and Cu concentrations. Positive correlation between La and La/Yb ratios for the diorites (Fig. 11a) is indicative of extensive

Table 4
Comparison of variable digestion techniques for PGE analyses.

Techniques	Sample mass (g)	Instrument	Recovery	Detection limits/blank	Reference
Lead FA	15	INAA, AAS, ICP-OES, ICP-MS		Au: 2 ng/g; Pt: 0.1 ng/g Pd: 0.5 ng/g	Hall and Pelchat (1994)
NiS FA		ICP-MS	–	Rh: 0.01 ng/g; Ir: 0.39 ng/g	Sun et al. (1998)
NiS FA	20	ICP-MS	96.7%	0.06 ng(Rh)–4.4 ng(Ru) (blank)	Oguri et al. (1999)
NiS FA	15	ICP-MS	86–98%	Ir: 0.07 ng/g; Au: 0.7 ng/g; Other PGEs: <0.15 ng/g	Jackson et al. (1990)
ID-NiS FA	10	N-TIMS, ICP-MS	–	Pd: 43 pg/g; Pt: 50 pg/g; Os: 4.2 pg/g; Ir: 3.8 pg/g (blank)	Ravizza and Pyle (1997)
NiS FA	10–50	LA-ICP-MS	–	10–90 ng/g	Jarvis et al. (1995)
Microwave acid digestion	1	ICP-MS	10–90%	0.2 μg/g (Rh)–1.1 μg/g (Pd)	Totland et al. (1995)
Acid digestion in bomb	10	ICP-MS	50–100%	4 pg/g (Ir)–14 pg/g (Pt)	Qi et al. (2011)
Carius tube	Up to 10	ICP-MS	–	1–15 pg/g	Rehkämper et al. (1998)
Carius tube in autoclave	Up to 12	ICP-MS	~100%	0.2 pg/g (Os)–18 pg/g (Pd)	Qi et al. (2007)
HPA-S	1	MC-ICP-MS	–	13 pg/g (Os)–0.77 ng/g (Pt)	Meisel et al. (2001)
Reusable Carius tube	1–5	ICP-MS	>90%	2 pg (Os)–0.25 ng (Pd) (blank)	Qi et al. (2013)

differentiation of the magmas. However, the poor correlation between PGE (e.g. Pd) and La/Yb (Fig. 11b) or Cu/Zr (Fig. 11c) suggests that the variation of PGE contents was not controlled by the fractionation of silicate minerals and Cu-sulfide. In addition, diorites have highly variable Cu/Pd ratios and Cu contents which are not correlated with Pd contents (Fig. 11d), likely indicating that Cu and Pd have different solubility in the fluids. It was indicated that Pt and Pd have significant solubility (>1 ppb) in low to moderate temperatures fluids which is highly oxidized (hematite stable), highly saline (>3 m NaCl), and/or acidic (pH < 4) (Gammons et al., 1992). However, fluid inclusions studies indicate that ore-forming fluids of the Tuwu deposit are in low temperature (100–200 °C) and in low to moderate salinity (0.35–15% NaCl equivalent) (Han et al., 2006; Liu et al., 2009), and the presence of CH_4, trace CO in the gas and SO_4^{2-} and NO_3^- in the solution is indicative of slightly oxidized conditions (Liu et al., 2009). Under such conditions, PGE could be very less soluble (<1 ppt) in these fluids (Gammons et al., 1992). Therefore, PGEs in diorite porphyries may not be modified by late PGE-poor fluids, and their concentrations should be original. As such, relatively uniform Pd but variable La/Yb ratios of diorite porphyries (Fig. 11b) suggested that parental magmas are relatively reduced and have reached sulfide saturation before the crystallization of silicate minerals. Sulfur contents of parental magmas are low so that the magmas can only generate small amounts of sulfide droplets. Such sulfide droplets could be homogeneously distributed in the parental magmas, resulting in uniform PGE contents in later formed diorite porphyries.

La contents of plagiogranite porphyries are also positively correlated with La/Yb ratios (Fig. 11a), consistent with fractional crystallization. Their PGE contents (e.g. Pd) show roughly negative correlations with La/Yb ratios as an index of the fractionation of silicate minerals (Fig. 11b), suggesting that PGEs are enriched in early-formed phases. However, Pd is positively correlated with Cu/Zr ratios, indicating that PGE contents of plagiogranite porphyries are dominantly controlled by sulfides (Fig. 11c). Given that Pd and Cu have very different partition coefficient in sulfides, the nearly uniform Cu/Pd ratios (5,100,000 to 7,800,000) of plagiogranite porphyries indicated that Cu-rich sulfides in these samples have precipitated nearly at the same time (Fig. 11d). Thus, such Cu-rich sulfides cannot be formed during the differentiation of silicate magmas because such progress would segregate sulfide with highly variable Cu/Pd ratios (e.g. Gao et al., 2012). Thus, parental magmas of plagiogranite porphyries were not sulfide-saturated before silicate mineral crystallization and sulfides were formed from hydrothermal fluids, possibly due to relative oxidized state of silicate magmas. In addition, Plagiogranite porphyries bear biotite with high MgO contents and Mg/(Mg + Fe + Mn) ratios of 0.35 to 0.60 (Rui et al., 2001) and contain large amounts of hematite and magnetite in ores, supportive of formation under high-fO_2 conditions.

Therefore, due to different water contents of parental magmas, parental magmas of diorites were relatively reduced, whereas those of plagiogranites were relatively oxidized with high sulfur contents. It is clear that the Cu mineralization was genetically related to the late-magmatic stage during the formation of plagiogranites. Cu, Au and PGEs were gradually enriched in residual fluids until the deposition of a large amount of sulfides (e.g. chalcopyrite). The plagiogranite-related ore-forming fluids have also altered the early diorites where disseminated Cu-sulfides precipitated.

5.5. Multi-stage mineralization and later hydrothermal overprinting

Cu-mineralized plagiogranite porphyries have Re–Os model ages of 189–195 Ma, much younger than the molybdenite Re–Os age of 323–343 Ma (Rui et al., 2002; Zhang et al., 2004) and zircon U–Pb age of 332–334 Ma (Chen et al., 2005; Liu et al., 2003; Shen et al., 2014b). Such a discrepancy may be related to the involvement of multiple hydrothermal events and/or open behavior of the Re–Os system.

The Tuwu Cu deposit is characterized by multi-stages of alteration as represented by different mineral associations (Han et al., 2006; Shen et al., 2014b; Zhang et al., 2006b). All plagiogranite porphyries in this study are copper mineralized, and sulfides were likely formed at the

Table 5
Advantages and disadvantages of digestion techniques for measuring PGE in porphyry Cu deposits.

Technique	Advantage	Disadvantage
Fire assay	1. All PGEs can be collected by fire assay technique; 2. Large sample sizes can reduce nugget effect; 3. The NiS button can be analyzed directly using laser ablation-ICP-MS.	1. Low recovery (<90%), particularly for Os and Au; 2. Some PGEs may be lost as Cl-bearing phases during the dissolution of NiS bead with HCl; 3. Relatively high procedure blank due to large mass of reagents used, especially for nickel powder.
Acid digestion	1. Purification of all acid is possible so that the blank levels are very low; 2. Acid digestion is proved to be more rapid and economical than FA technique.	1. The small sample size (0.5–5 g) will result in poor reproducibility due to the nugget effect; 2. Refractory minerals might not be completely decomposed by acid digestion; 3. Carius tube may explode under high temperature and pressure; 4. HPA-S analysis is costly.

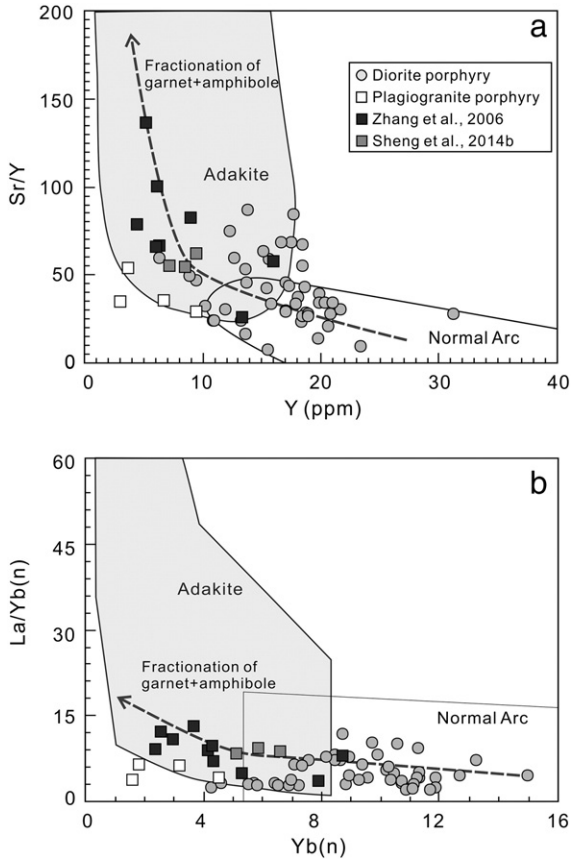

Fig. 10. Plots of (a) Sr/Y vs Y and (b) La/Yb(n) vs Yb(n) for the diorite and plagiogranite porphyries from the Tuwu deposit (Modified after Defant and Drummond, 1990).

same stage. On the other hand, diorite porphyries formed earlier and were partially overprinted by the later copper mineralization. The Re–Os isotopic compositions of porphyritic rocks at Tuwu can be used to evaluate the behavior of Re–Os system in such multi-stage alterations. Diorites have highly variable Re (0.073–15.3 ppb) and Os contents (0.006–0.097 ppb), resulting in highly variable $^{187}Re/^{188}Os$ ratios, some of which exceed 2000 and could be considered as "LLHR" Stein et al. (2000). Samples with low $^{187}Re/^{188}Os$ ratios (<2000) yield an isochron age of 259 Ma, older than that of all samples (218 Ma), but have initial $^{187}Os/^{188}Os$ ratios (0.21) lower than those of all samples (0.34) (Fig. 9a). Such a Re–Os isotopic feature suggests that relatively high Os samples have Os isotopic compositions near to the mantle, but low Os and high Re samples have more radiogenic Os and are mostly crustal in origin. In addition, Re of diorite porphyries has a roughly negative correlation with Os, supportive of different origins of Re and Os.

Re of diorite porphyries is positively correlated with Cu, Au, and Mo (Fig. 12a–c), suggesting that the enrichment of Re is closely associated with the Cu–Mo–Au mineralization at Tuwu. However, Re and As do not show an expected positive correlation, which cannot be explained by a single hydrothermal event. High As samples only locally distributed in the deposits and commonly contain enargite at the margin of or as inclusions in chalcopyrite (Figs. 3f; 4e–f), suggesting that the As-rich and Re-poor sulfide minerals postdate the dominant copper mineralization (As-poor and Re-rich). In addition, enargite have been reported in many porphyry deposits as low temperature products in the late-stage of Cu–Au mineralization (Chouinard et al., 2005; Khashgerel et al., 2006; Muntean and Einaudi, 2001). Thus, the continuous distribution of As and Re on the plot was likely generated by the mixing of the early As-poor and Re-rich fluids with later As-rich and Re-poor solutions.

It is noted that plagiogranites and diorites have a weighted average Re–Os model age of 192 ± 22 Ma and 223 ± 14 Ma, respectively, younger than the molybdenite Re–Os age (322 Ma) of the Tuwu deposit Stein et al. (2000); (Rui et al., 2002). These samples have very high

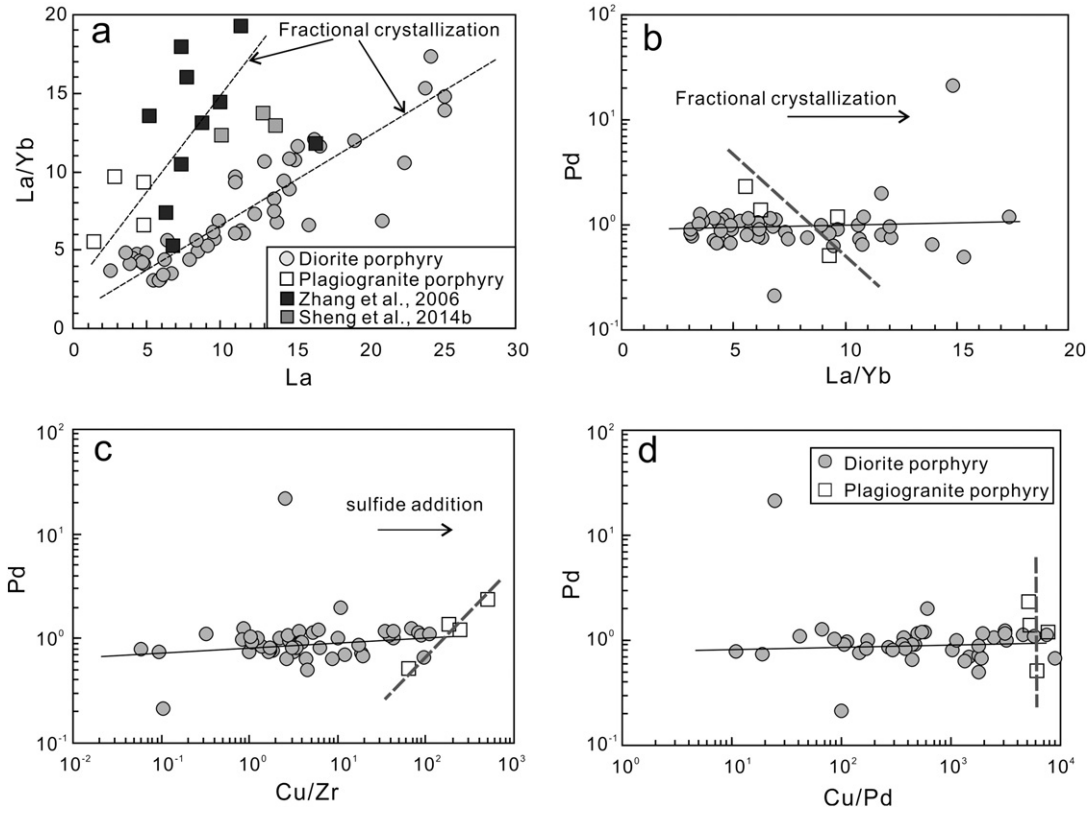

Fig. 11. Plots of (a) La vs La/Yb; (b) La/Yb vs Pd; (c) Cu/Zr vs Pd; (d) Cu/Pd ratios vs Pd for Tuwu porphyries, showing different fractionation histories of diorite and plagiogranite porphyries.

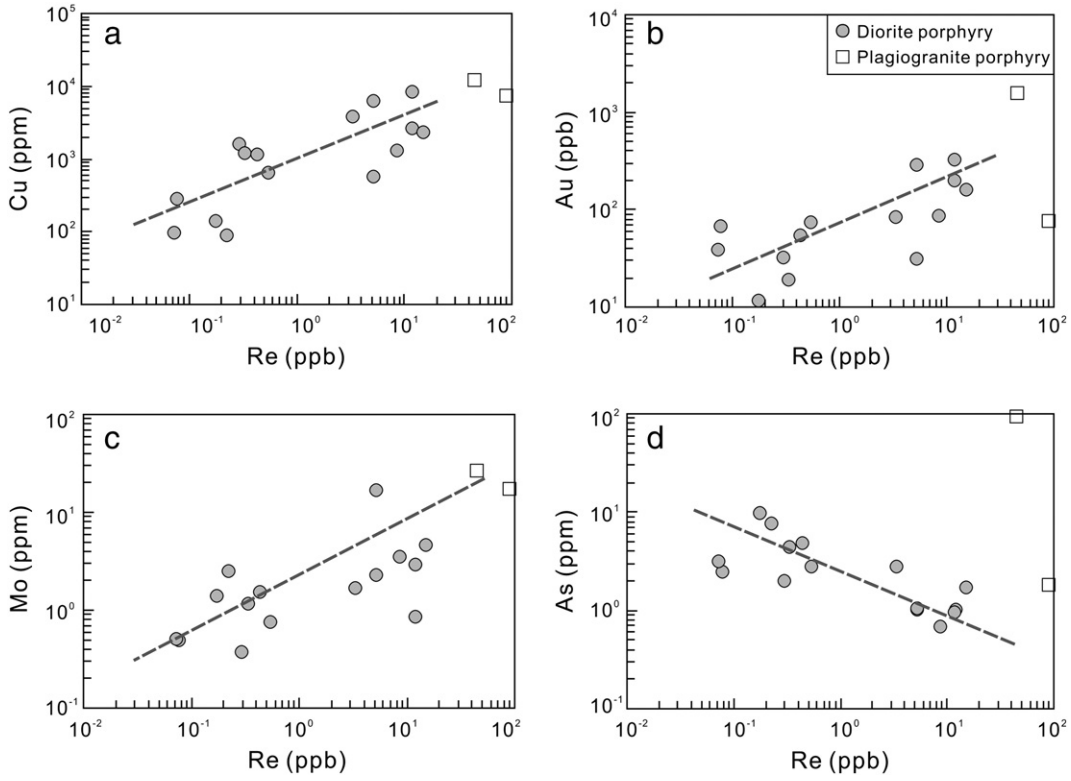

Fig. 12. Binary plots of (a) Re vs Cu; (b) Re vs Au; (c) Re vs As; and (d) Re vs Mo, indicating that a later stage depletion of Re is associated with Cu–Mo–(Au) mineralization.

$^{187}Re/^{188}Os$ ratios (mostly >4000), and thus the contribution of common Os in these samples in the calculation of model ages is negligible. The younger model age for these rocks may be caused by loss of Re due to overprint of later hydrothermal fluids. Indeed, there are some younger granitic plutons (e.g. the 257 Ma Longdong granite) (Zhou et al., 2010) and related deposits (e.g. the 225 Ma Baishan Mo deposit) (Zhang et al., 2005) in the region. It is possible that the Re–Os system of the Tuwu deposit was modified by the thermal activities related to these magmatic events (e.g. leaching Re) at Tuwu.

Thus, the bulk rock Re–Os isotopic compositions for the porphyries in Tuwu are consistent with at least two stages of copper mineralization. The early stage of copper mineralization was generated by fluids relatively enriched in Re, Mo and Au; whereas the later stage is characterized by the enrichment of As and depletion of Re (Fig. 13). Both

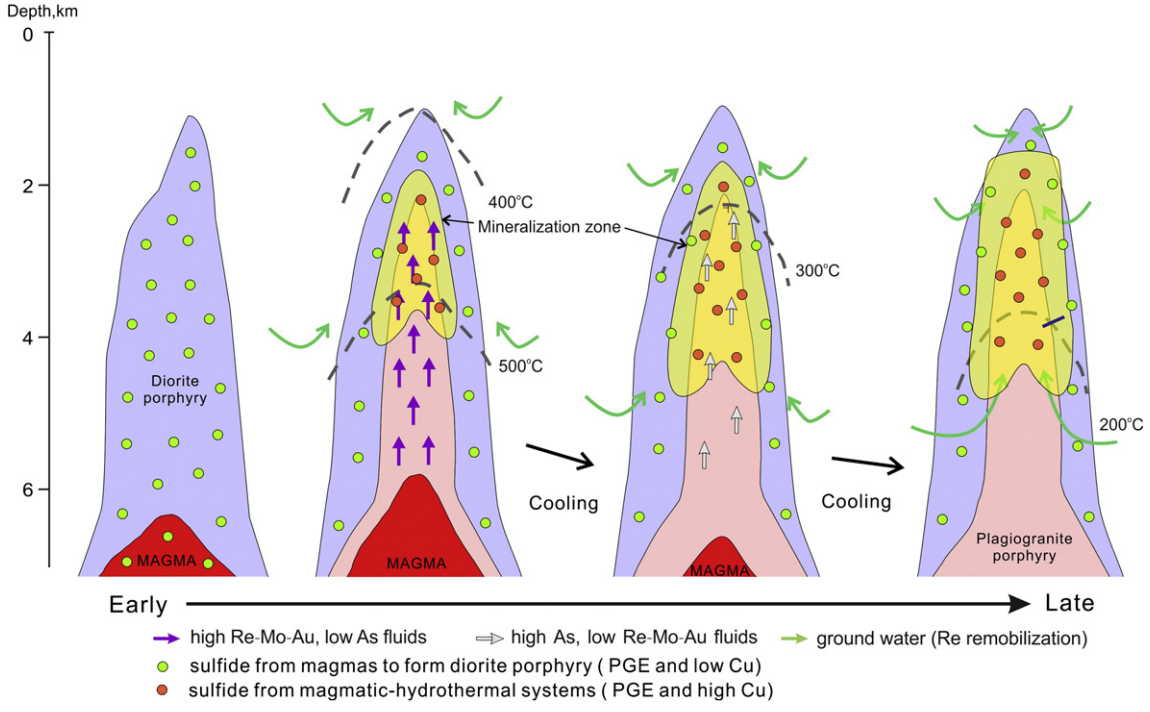

Fig. 13. A simplified genetic model of the Tuwu porphyry Cu deposit showing the evolution of the magmatic-hydrothermal system (Revised from Sillitoe, 2010).

stages of the copper mineralization were overprinted by later hydrothermal fluids that were likely able to leach Re to result in younger whole Re–Os model ages (Fig. 13).

6. Conclusions

The principal conclusions of this study are as follows:

1. PGEs in pre-mineralized diorite porphyries at Tuwu remained immobile during later alteration in the porphyry magmatic-hydrothermal system so that the PGE geochemistry could be used to examine the magma evolution of the diorite porphyries.
2. Both diorite and plagiogranite porphyries are derived from magmas generated by partial melting of a wet mantle wedge with different water contents. Parental magmas of diorite porphyries have reached sulfide saturation before fractional crystallization of silicate minerals, whereas magmas of plagiogranite porphyries gained sulfide saturation in magmatic-hydrothermal stage.
3. There are two stages of the Cu mineralization in the Tuwu deposit: the first stage is characterized by relatively high Au, Mo and Re; whereas hydrothermal fluids in the later stage were enriched in As and depleted in Re.
4. The Re–Os system in porphyry rocks at Tuwu was modified by younger hydrothermal fluids, by which Re was leached.

Acknowledgment

This study was supported by grants from the Research Grant Council of Hong Kong (HKU7064/13P), and a 12th Five-Year Plan Project of State Key Laboratory of Ore Deposit Geochemistry, Chinese Academy of Sciences (SKLODG-ZY125-02). We are very grateful to Dr. Wei Wang from the University of Hong Kong and Prof. Jianjun Lu and Miss Wei Pu from the Nanjing University for the lab assistant. Mr. Gang Deng, and Mr. Youfeng Liu of the Sixth Team of the Geological Survey of Xinjiang, Miss Li Xie of the Yanxin Copper Mining Company were thanked for very capable field assistant. We are grateful to the guest editor and two reviewers for the constructive comments for the improvement of the manuscript.

Appendix 1

sample	TWG901	TWG902	TWG903	TWG904	TWG905	TWG907	TWG908	TWG909	TWG910
Lithology	DP	DP	DP	DP	DP	DP	DP	DP	DP
Major elemental oxides (wt.%)									
SiO2	56.8	59.3	55.1	56.3	59.3	58.2	60.7	60.0	55.6
TiO2	1.13	1.17	1.12	1.17	1.17	1.09	1.00	1.12	0.96
Al2O3	17.61	15.67	17.91	16.66	15.69	17.63	15.52	15.90	15.73
Fe2O3	10.25	8.37	9.83	8.87	7.73	9.56	7.90	7.55	8.72
MnO	0.11	0.12	0.08	0.11	0.13	0.07	0.09	0.07	0.09
MgO	5.86	6.4	7.29	7.92	7.05	5.6	6.43	6.03	7.61
CaO	4.17	3.88	3.7	4.19	3.96	3.18	3.54	3.93	6.41
Na2O	3.62	4.68	4.37	4.08	4.35	3.99	4.06	5.11	4.35
K2O	0.15	0.02	0.38	0.36	0.23	0.24	0.44	0.05	0.27
P_2O_5	0.2	0.07	0.14	0.28	0.34	0.3	0.25	0.25	0.18
S	0.08	0.32	0.06	0.05	0.08	0.12	0.07	0.04	0.04
ALK	3.77	4.70	4.75	4.44	4.58	4.23	4.50	5.16	4.62
Trace elements (ppm)									
Sc	23.9	20.5	20.8	21.3	21.6	21.9	13.0	7.8	9.1
V	157	156	219	183	174	227	215	118	173
Cr	76	83	73	76	75	64	66	60	60
Co	22.4	16.7	21.8	27.9	20.5	18.4	17.4	19.6	16.4
Ni	84	89	63	62	59	48	161	90	73
Cu	342	294	269	261	434	604	445	229	171
Zn	71	112	96	130	125	67	55	78	50
Ga	18.1	14.0	18.7	17.6	16.2	16.6	15.7	11.3	16.6
As	2.68	2.00	2.44	3.4	1.95	2.03	2.37	2.42	1.99
Rb	4.1	1.59	10.6	10.4	6.8	6.6	12.6	2.28	6.0
Sr	646	273	780	756	587	426	625	438	1016
Y	21.2	19.8	17.0	17.3	20.8	18.3	13.7	20.6	18.4
Zr	153	161	157	158	155	140	139	168	137
Nb	4.9	4.7	4.5	4.9	4.6	4.2	3.9	5.0	3.6
Mo	0.23	0.14	0.17	0.23	0.19	0.24	0.20	0.10	0.38
Cd	0.15	0.28	0.21	0.18	0.24	0.14	0.17	0.22	0.56
Cs	0.85	0.34	1.07	0.94	0.64	1.16	1.34	0.26	1.61
Ba	49	16.0	57	56	53	38	49	12.3	46
La	22.5	5.9	13.6	11.4	13.8	25.2	13.0	12.3	9.6
Ce	55	15.2	33	28.0	35	57	39	32.2	25.0
Pr	7.2	2.26	4.2	3.7	4.8	7.1	3.9	4.2	3.4
Nd	28.8	10.3	17.8	16.1	19.7	29.2	16.9	18.7	15.1
Sm	5.4	2.93	3.9	3.7	4.2	5.5	3.4	4.0	3.8
Eu	1.35	0.78	1.00	0.99	1.16	1.11	0.72	1.01	1.17
Gd	4.8	3.5	3.7	3.5	4.1	4.8	2.84	3.8	3.5
Tb	0.79	0.63	0.58	0.61	0.69	0.72	0.41	0.61	0.57
Dy	4.2	3.7	3.0	3.2	3.7	3.7	2.12	3.4	3.2
Ho	0.85	0.77	0.67	0.68	0.81	0.73	0.46	0.75	0.69
Er	2.31	2.14	1.82	1.93	2.28	1.99	1.22	1.90	1.79
Tm	0.33	0.30	0.25	0.27	0.32	0.28	0.17	0.27	0.25

Appendix 1 (*continued*)

sample	TWG901	TWG902	TWG903	TWG904	TWG905	TWG907	TWG908	TWG909	TWG910
Lithology	DP	DP	DP	DP	DP	DP	DP	DP	DP
Trace elements (ppm)									
Yb	2.13	1.88	1.64	1.82	2.04	1.81	1.22	1.68	1.66
Lu	0.29	0.26	0.24	0.26	0.29	0.25	0.18	0.25	0.24
Hf	3.6	3.9	3.6	3.8	3.6	3.2	3.0	3.6	3.0
Ta	0.31	0.33	0.32	0.34	0.31	0.32	0.25	0.31	0.26
Pb	9.6	3.9	6.4	14.8	3.2	5.9	4.7	6.9	5.1
Bi	0.03	0.03	0.04	0.06	0.15	0.03	0.11	0.07	0.03
Th	1.64	1.45	1.70	1.57	1.74	1.75	1.01	1.10	0.73
U	0.59	0.65	0.53	0.64	0.74	0.64	0.54	0.56	0.46

References

Alonso-Perez, R., Müntener, O., Ulmer, P., 2009. Igneous garnet and amphibole fractionation in the roots of island arcs: experimental constraints on andesitic liquids. Contrib. Mineral. Petrol. 157, 541–558.

Archibald, S.M., Migdisov, A.A., Williams-Jones, A.E., 2002. An experimental study of the stability of copper chloride complexes in water vapor at elevated temperatures and pressures. Geochim. Cosmochim. Acta 66, 1611–1619.

Asif, M., Parry, S.J., 1991. Study of the digestion of chromite during nickel sulphide fire assay for the platinum group elements and gold. Analyst 116, 1071–1073.

Azaroual, M., Romand, B., Freyssinet, P., Disnar, J.-R., 2001. Solubility of platinum in aqueous solutions at 25 °C and pHs 4 to 10 under oxidizing conditions. Geochim. Cosmochim. Acta 65, 4453–4466.

Ballard, J.R., Palin, J.M., Campbell, I.H., 2002. Relative oxidation states of magmas inferred from Ce(IV)/Ce(III) in zircon: application to porphyry copper deposits of northern Chile. Contrib. Mineral. Petrol. 144, 347–364.

Barefoot, R.R., Van Loon, J.C., 1999. Recent advances in the determination of the platinum group elements and gold. Talanta 49, 1–14.

Barnes, S.-J., Lightfoot, P.C., 2005. Formation of Magmatic Nickel Sulfide Ore Deposits and Processes Affecting Their Copper and Platinum Group Element Contents. Econ. Geol. 100th Annversary Volume. pp. 179–214.

Barnes, S.J., Liu, W., 2012. Pt and Pd mobility in hydrothermal fluids: evidence from komatiites and from thermodynamic modelling. Ore Geol. Rev. 44, 49–58.

Barnes, S.-J., Maier, W.D., 1999. The Fractionation of Ni, Cu and the Noble Metals in Silicate and Sulfide Liquids. In: Keays, R.R., Lesher, C.M., Lightfoot, P.C., Farrow, C.E.G. (Eds.), Dynamic Processes in Magmatic Ore Deposits and their application in mineral exploration. Geological Association of Canada, Short Course Notes, pp. 69–106.

Bézos, A., Lorand, J.P., Humler, E., Gros, M., 2005. Platinum-group element systematics in Mid-Oceanic Ridge basaltic glasses from the Pacific, Atlantic, and Indian Oceans. Geochim. Cosmochim. Acta 69, 2613–2627.

Cao, M., Qin, K., Li, G., Jin, L., Evans, N.J., Yang, X., 2014a. Baogutu: an example of reduced porphyry Cu deposit in western Junggar. Ore Geol. Rev. 56, 159–180.

Cao, M., Qin, K., Li, G., Yang, Y., Evans, N.J., Zhang, R., Jin, L., 2014b. Magmatic process recorded in plagioclase at the Baogutu reduced porphyry Cu deposit, western Junggar, NW-China. J. Asian Earth Sci. 82, 136–150.

Chen, F., Li, H., Chen, Y., Wang, D., Wang, J., Liu, D., Tang, Y., Zhou, R., 2005. Zircon SHRIMP U–Pb dating and its geological significance of mineralization in Tuwu–Yandong porphyry copper mine, east Tianshan mountain. Acta Geol. Sin. 79, 256–261.

Chiaradia, M., Müntener, O., Beate, B., Fontignie, D., 2009. Adakite-like volcanism of Ecuador: lower crust magmatic evolution and recycling. Contrib. Mineral. Petrol. 158, 563–588.

Chouinard, A., Williams-Jones, A.E., Leonardson, R.W., Hodgson, C.J., Silva, P., Téllez, C., Vega, J., Rojas, F., 2005. Geology and genesis of the multistage high-sulfidation epithermal Pascua Au–Ag–Cu deposit, Chile and Argentina. Econ. Geol. 100, 463–490.

Coldwell, B., Adam, J., Rushmer, T., Macpherson, C.G., 2011. Evolution of the East Philippine Arc: experimental constraints on magmatic phase relations and adakitic melt formation. Contrib. Mineral. Petrol. 162, 835–848.

Coleman, R.G., 1989. Continental growth of Northwest China. Tectonics 8, 621–635.

Cooke, D.R., Hollings, P., Walshe, J.L., 2005. Giant porphyry deposits: characteristics, distribution, and tectonic controls. Econ. Geol. 100, 801–818.

Davidson, J., Turner, S., Handley, H., Macpherson, C., Dosseto, A., 2007. Amphibole "sponge" in arc crust? Geology 35, 787–790.

Defant, M.J., Drummond, M.S., 1990. Derivation of some modern arc magmas by melting of young subducted lithosphere. Nature 347, 662–665.

Economou-Eliopoulos, M., Eliopoulos, D.G., 2000. Palladium, platinum and gold concentration in porphyry copper systems of Greece and their genetic significance. Ore Geol. Rev. 16, 59–70.

Eliopoulos, D.G., Economou-Eliopoulos, M., 1991. Platinum-group element and gold contents in the Skouries porphyry copper-deposit, Chalkidiki peninsula, Northern Greece. Econ. Geol. 86, 740–749.

Fleet, M.E., Stone, W.E., Crocket, J.H., 1991. Partitioning of palladium, iridium, and platinum between sulfide liquid and basalt melt: effects of melt composition, concentration, and oxygen fugacity. Geochim. Cosmochim. Acta 55, 2545–2554.

Fleet, M.E., Crocket, J.H., Liu, M.H., Stone, W.E., 1999. Laboratory partitioning of platinum-group elements (PGE) and gold with application to magmatic sulfide-PGE deposits. Lithos 47, 127–142.

Gammons, C.H., 1995. Experimental investigations of the hydrothermal geochemistry of platinum and palladium: IV. The stoichiometry of Pt(IV) and Pd(II) chloride complexes at 100 to 300 °C. Geochim. Cosmochim. Acta 59, 1655–1667.

Gammons, C.H., 1996. Experimental investigations of the hydrothermal geochemistry of platinum and palladium: V. Equilibria between platinum metal, Pt(II), and Pt(IV) chloride complexes at 25 to 300 °C. Geochim. Cosmochim. Acta 60, 1683–1694.

Gammons, C.H., Bloom, M.S., 1993. Experimental investigation of the hydrothermal geochemistry of platinum and palladium: II. The solubility of PtS and PdS in aqueous sulfide solutions to 300 °C. Geochim. Cosmochim. Acta 57, 2451–2467.

Gammons, C.H., Bloom, M.S., Yu, Y., 1992. Experimental investigation of the hydrothermal geochemistry of platinum and palladium: I. Solubility of platinum and palladium sulfide minerals in $NaCl/H_2SO_4$ solutions at 300 °C. Geochim. Cosmochim. Acta 56, 3881–3894.

Gao, J.-F., Zhou, M.-F., 2013. Generation and evolution of siliceous high magnesium basaltic magmas in the formation of the Permian Huangshandong intrusion (Xinjiang, NW China). Lithos 162–163, 128–139.

Gao, J., Li, M.S., Xiao, X.C., Tang, Y.Q., He, G.Q., 1998. Paleozoic tectonic evolution of the Tianshan Orogen, northwestern China. Tectonophysics 287, 213–231.

Gao, J.F., Lu, J.J., Lai, M.Y., Lin, Y.P., Pu, W., 2003. Analysis of trace elements in rock samples using HR-ICPMS. J. Nanjing Univ. (Nat. Sci.) 39, 844–850.

Gao, J.F., Zhou, M.F., Lightfoot, P.C., Wang, C.Y., Qi, L., 2012. Origin of PGE-poor and Cu-rich magmatic sulfides from the Kalatongke deposit, Xinjiang, NW China. Econ. Geol. 107, 481–506.

Gao, J.-F., Zhou, M.-F., Lightfoot, P.C., Wang, C.Y., Qi, L., Sun, M., 2013. Sulfide saturation and magma emplacement in the formation of the Permian Huangshandong Ni–Cu sulfide deposit, Xinjiang, Northwestern China. Econ. Geol. 108, 1833–1848.

Gowing, C.J.B., Potts, P.J., 1991. Evaluation of a rapid technique for the determination of precious metals in geological samples based on a selective aqua regia leach. Analyst 116, 773–779.

Gros, M., Lorand, J.-P., Luguet, A., 2002. Analysis of platinum group elements and gold in geological materials using NiS fire assay and Te coprecipitation; the NiS dissolution step revisited. Chem. Geol. 185, 179–190.

Hack, A.C., Mavrogenes, J.A., 2006. A synthetic fluid inclusion study of copper solubility in hydrothermal brines from 525 to 725 °C and 0.3 to 1.7 GPa. Geochim. Cosmochim. Acta 70, 3970–3985.

Hall, G.E.M., Pelchat, J.C., 1994. Analysis of geological materials for gold, platinum and palladium at low ppb levels by fire assay-ICP mass spectrometry. Chem. Geol. 115, 61–72.

Han, C.M., Xiao, W.J., Zhao, G., Mao, J.W., Yang, J.M., Wang, Z.L., Yan, Z., Mao, Q.Q., 2006. Geological characteristics and genesis of the Tuwu porphyry copper deposit, Hami, Xinjiang, Central Asia. Ore Geol. Rev. 29, 77–94.

Hanley, J.J., 2005. The Aqueous Geochemistry of the Platinum-group Elements (PGE) in Surficial, Low-T Hydrothermal and High-T Magmatic-hydrothermal Environments. In: Mungall, J.E. (Ed.), Exploration for Platinum-group element deposits. Mineral. Assoc. Canada, Short Course, pp. 35–56.

Hassler, D.R., Peucker-Ehrenbrink, B., Ravizza, G.E., 2000. Rapid determination of Os isotopic composition by sparging OsO_4 into a magnetic-sector ICP-MS. Chem. Geol. 166, 1–14.

Hoffman, E.L., Naldrett, A.J., Van Loon, J.C., Hancock, R.G.V., Manson, A., 1978. The determination of all the platinum group elements and gold in rocks and ore by neutron activation analysis after preconcentration by a nickel sulphide fire-assay technique on large samples. Anal. Chim. Acta. 102, 157–166.

Hou, Z.Q., Gao, Y.F., Qu, X.M., Rui, Z.Y., Mo, X.X., 2004. Origin of adakitic intrusives generated during mid-Miocene east–west extension in southern Tibet. Earth Planet. Sci. Lett. 220, 139–155.

Hou, G.S., Tang, H.F., Liu, C.Q., Wang, Y.B., 2005. Geochronological and geochemical study on the wallrock of Tuwu–Yandong porphyry copper deposits, eastern Tianshan mountains. Acta Petrol. Sin. 21, 1729–1736.

Hou, Z., Yang, Z., Qu, X., Meng, X., Li, Z., Beaudoin, G., Rui, Z., Gao, Y., Zaw, K., 2009. The Miocene Gangdese porphyry copper belt generated during post-collisional extension in the Tibetan Orogen. Ore Geol. Rev. 36, 25–51.

Jackson, S.E., Fryer, B.J., Gosse, W., Healey, D.C., Longerich, H.P., Strong, D.F., 1990. Determination of the precious metals in geological materials by inductively coupled plasma-mass spectrometry (ICP-MS) with nickel sulphide fire-assay collection and tellurium coprecipitation. Chem. Geol. 83, 119–132.

Jarvis, K.E., Williams, J.G., Parry, S.J., Bertalan, E., 1995. Quantitative determination of the platinum-group elements and gold using NiS fire assay with laser ablation-inductively coupled plasma-mass spectrometry (LA-ICP-MS). Chem. Geol. 124, 37–46.
Juvonen, R., Lakomaa, T., Soikkeli, L., 2002. Determination of gold and the platinum group elements in geological samples by ICP-MS after nickel sulphide fire assay: difficulties encountered with different types of geological samples. Talanta 58, 595–603.
Kay, R.W., 1978. Aleutian magnesian andesites: melts from subducted Pacific ocean crust. J. Volcanol. Geotherm. Res. 4, 117–132.
Kelley, K.A., Cottrell, E., 2009. Water and the oxidation state of subduction zone magmas. Science 325, 605–607.
Kelley, K.A., Plank, T., Newman, S., Stolper, E.M., Grove, T.L., Parman, S., Hauri, E.H., 2010. Mantle melting as a function of water content beneath the Mariana Arc. J. Petrol. 51, 1711–1738.
Khashgerel, B.-E., Rye, R.O., Hedenquist, J.W., Kavalieris, I., 2006. Geology and reconnaissance stable isotope study of the Oyu Tolgoi porphyry Cu–Au system, South Gobi, Mongolia. Econ. Geol. 101, 503–522.
Li, J.W., Zhao, X.F., Zhou, M.F., Vasconcelos, P., Ma, C.Q., Deng, X.D., de Souza, Z.S., Zhao, Y. X., Wu, G., 2008. Origin of the Tongshankou porphyry-skarn Cu–Mo deposit, eastern Yangtze craton, Eastern China: geochronological, geochemical, and Sr–Nd–Hf isotopic constraints. Mineral. Deposita 43, 315–336.
Li, J., Jiang, X.-Y., Xu, J.-F., Zhong, L.-F., Wang, X.-C., Wang, G.-Q., Zhao, P.-P., 2014. Determination of platinum-group elements and Re–Os isotopes using ID-ICP-MS and N-TIMS from a single digestion after two-stage column separation. Geostand. Geoanal. Res. 38, 37–50.
Liu, W., McPhail, D.C., 2005. Thermodynamic properties of copper chloride complexes and copper transport in magmatic-hydrothermal solutions. Chem. Geol. 221, 21–39.
Liu, D., Chen, Y., Wang, D., Tang, Y., Zhou, R., Wang, J., Li, H., Chen, F., 2003. A discussion on problems related to mineralization of Tuwu–Yandong Cu–Mo Ore-field in Hami, Xinjiang. Mineral Deposits 22, 344–358.
Liu, M., Wang, Z.L., Zhang, Z.H., Chen, W.S., Yang, D., 2009. Fluid inclusion geochemistry of Tuwu porphyry copper deposit, eastern Tianshan in Xinjiang. Acta Petrol. Sin. 25, 1446–1455.
Macpherson, C.G., Dreher, S.T., Thirlwall, M.F., 2006. Adakites without slab melting: high pressure differentiation of island arc magma, Mindanao, the Philippines. Earth Planet. Sci. Lett. 243, 581–593.
Martin, H., 1999. Adakitic magmas: modern analogues of Archaean granitoids. Lithos 46, 411–429.
Martin, H., Smithies, R.H., Rapp, R., Moyen, J.F., Champion, D., 2005. An overview of adakite, tonalite–trondhjemite–granodiorite (TTG), and sanukitoid: relationships and some implications for crustal evolution. Lithos 79, 1–24.
McDonough, W.F., Sun, S.s., 1995. The composition of the Earth. Chem. Geol. 120, 223–253.
Meisel, T., Moser, J., 2004. Reference materials for geochemical PGE analysis: new analytical data for Ru, Rh, Pd, Os, Ir, Pt and Re by isotope dilution ICP-MS in 11 geological reference materials. Chem. Geol. 208, 319–338.
Meisel, T., Moser, J., Wegscheider, W., 2001. Recognizing heterogeneous distribution of platinum group elements (PGE) in geological materials by means of the Re–Os isotope system. Fresenius J. Anal. Chem. 370, 566–572.
Meisel, T., Fellner, N., Moser, J., 2003. A simple procedure for the determination of platinum group elements and rhenium (Ru, Rh, Pd, Re, Os, Ir and Pt) using ID-ICP-MS with an inexpensive on-line matrix separation in geological and environmental materials. J. Anal. At. Spectrom. 18, 720–726.
Moser, J., Wegscheider, W., Meisel, T., Fellner, N., 2003. An uncertainty budget for trace analysis by isotope-dilution ICP-MS with proper consideration of correlation. Anal. Bioanal. Chem. 377, 97–110.
Mountain, B.W., Wood, S.A., 1988. Chemical controls on the solubility, transport and deposition of platinum and palladium in hydrothermal solutions; a thermodynamic approach. Econ. Geol. 83, 492–510.
Moyen, J.-F., 2009. High Sr/Y and La/Yb ratios: the meaning of the "adakitic signature". Lithos 112, 556–574.
Muntean, J.L., Einaudi, M.T., 2001. Porphyry-epithermal transition: Maricunga Belt, Northern Chile. Econ. Geol. 96, 743–772.
Müntener, O., Ulmer, P., 2006. Experimentally derived high-pressure cumulates from hydrous arc magmas and consequences for the seismic velocity structure of lower arc crust. Geophys. Res. Lett. 33, L21308.
Müntener, O., Kelemen, P., Grove, T., 2001. The role of H_2O during crystallization of primitive arc magmas under uppermost mantle conditions and genesis of igneous pyroxenites: an experimental study. Contrib. Mineral. Petrol. 141, 643–658.
Naldrett, A.J., 2004. Magmatic Sulfide Deposit: Geology, Geochemistry and Exploration. Springer, Heidelberg Berlin New York.
Nicholls, I., Ringwood, A., 1973. Effect of water on olivine stability in tholeiites and the production of silica-saturated magmas in the island-arc environment. J. Geol. 285–300.
Oguri, K., Shimoda, G., Tatsumi, Y., 1999. Quantitative determination of gold and the platinum-group elements in geological samples using improved NiS fire-assay and tellurium coprecipitation with inductively coupled plasma-mass spectrometry (ICP-MS). Chem. Geol. 157, 189–197.
Oyarzun, R., Marquez, A., Lillo, J., Lopez, I., Rivera, S., 2001. Giant versus small porphyry copper deposits of Cenozoic age in northern Chile: adakitic versus normal calc-alkaline magmatism. Mineral. Deposita 36, 794–798.
Pan, P., Wood, S.A., 1994. Solubility of Pt and Pd sulfides and Au metal in aqueous bisulfide solutions. Mineral. Deposita 29, 373–390.
Parman, S.W., Grove, T.L., Kelley, K.A., Plank, T., 2011. Along-arc variations in the pre-eruptive H_2O contents of Mariana arc magmas inferred from fractionation paths. J. Petrol. 52, 257–278.
Pearson, D.G., Woodland, S.J., 2000. Solvent extraction/anion exchange separation and determination of PGEs (Os, Ir, Pt, Pd, Ru) and Re–Os isotopes in geological samples by isotope dilution ICP-MS. Chem. Geol. 165, 87–107.
Pu, W., Gao, J.F., Zhao, K.D., Ling, H.F., Jiang, S.Y., 2005. Separation method of Rb–Sr, Sm–Nd using DCTA and HIBA. J. Nanjing Univ. (Nat. Sci.) 41, 445–450.
Qi, L., Hu, J., Gregoire, D.C., 2000. Determination of trace elements in granites by inductively coupled plasma mass spectrometry. Talanta 51, 507–513.
Qi, L., Zhou, M.F., Wang, C.Y., 2004. Determination of low concentrations of platinum group elements in geological samples by ID-ICP-MS. J. Anal. At. Spectrom. 19, 1335–1339.
Qi, L., Zhou, M.F., Wang, C.Y., Sun, M., 2007. Evaluation of a technique for determining Re and PGEs in geological samples by ICP-MS coupled with a modified Carius tube digestion. Geochem. J. 41, 407–414.
Qi, L., Zhou, M.F., Gao, J.F., Zhao, Z., 2010. An improved Carius tube technique for determination of low concentrations of Re and Os in pyrites. J. Anal. At. Spectrom. 25, 585–589.
Qi, L., Gao, J., Huang, X., Hu, J., Zhou, M.-F., Zhong, H., 2011. An improved digestion technique for determination of platinum group elements in geological samples. J. Anal. At. Spectrom. 26, 1900–1904.
Qi, L., Gao, J.-F., Zhou, M.-F., Hu, J., 2013. The design of re-usable carius tubes for the determination of rhenium, osmium and platinum-group elements in geological samples. Geostand. Geoanal. Res. 37, 345–351.
Ravizza, G., Pyle, D., 1997. PGE and Os isotopic analyses of single sample aliquots with NiS fire assay preconcentration. Chem. Geol. 141, 251–268.
Rehkämper, M., Halliday, A.N., Wentz, R.F., 1998. Low-blank digestion of geological samples for platinum-group element analysis using a modified Carius Tube design. Fresenius J. Anal. Chem. 361, 217–219.
Richards, J.P., 2003. Tectono-magmatic precursors for porphyry Cu-(Mo–Au) deposit formation. Econ. Geol. 98, 1515–1533.
Richards, J.P., 2009. Postsubduction porphyry Cu–Au and epithermal Au deposits: products of remelting of subduction-modified lithosphere. Geology 37, 247–250.
Richards, J.P., 2011. High Sr/Y arc magmas and porphyry Cu ± Mo ± Au deposits: just add water. Econ. Geol. 106, 1075–1081.
RodrÍguez, C., Sellés, D., Dungan, M., Langmuir, C., Leeman, W., 2007. Adakitic dacites formed by intracrustal crystal fractionation of water-rich parent magmas at Nevado de Longaví Volcano (36·2°S; Andean Southern Volcanic Zone, Central Chile). J. Petrol. 48, 2033–2061.
Rowins, S.M., 2000. Reduced porphyry copper–gold deposits: a new variation on an old theme. Geology 28, 491–494.
Rui, Z., Wang, F., Li, H., Dong, L., Wang, L., Jiang, L., Liu, Y., Wang, L., Chen, W., 2001. Advance of the porphyry copper belt of the East Tienshan mountain, Xinjiang. Chin. Geol. 28, 11–16.
Rui, Z., Wang, L., Wang, Y., Liu, Y., 2002. Discussion on metallogenic epoch of Tuwu and Yandong porphyry copper deposits in eastern Tianshan Mountains, Xinjiang. Mineral Deposits 21, 22–33.
Sajona, F.G., Maury, R.C., 1998. Association of adakites with gold and copper mineralization in the Philippines. C. R. Acad Sci IIA - Earth Planet. Sci. 326, 27–34.
Sassani, D.C., Shock, E.L., 1998. Solubility and transport of platinum-group elements in supercritical fluids: summary and estimates of thermodynamic properties for ruthenium, rhodium, palladium, and platinum solids, aqueous ions, and complexes to 1000 °C and 5 kbar. Geochim. Cosmochim. Acta 62, 2643–2671.
Sattari, P., Brenan, J.M., Horn, I., McDonough, W.F., 2002. Experimental constraints on the sulfide- and chromite-silicate melt partitioning behavior of rhenium and platinum-group elements. Econ. Geol. Bull. Soc. Econ. Geol. 97, 385–398.
Savard, D., Barnes, S.-J., Meisel, T., 2010. Comparison between nickel–sulfur fire assay Te co-precipitation and isotope dilution with high-pressure asher acid digestion for the determination of platinum-group elements, rhenium and gold. Geostand. Geoanal. Res. 34, 281–291.
Schmidt, M.W., Poli, S., 1998. Experimentally based water budgets for dehydrating slabs and consequences for arc magma generation. Earth Planet. Sci. Lett. 163, 361–379.
Shen, P., Pan, H., Dong, L., 2014a. Yandong porphyry Cu deposit, Xinjiang, China—geology, geochemistry and SIMS U–Pb zircon geochronology of host porphyries and associated alteration and mineralization. J. Asian Earth Sci. 80, 197–217.
Shen, P., Pan, H., Zhou, T., Wang, J., 2014b. Petrography, geochemistry and geochronology of the host porphyries and associated alteration at the Tuwu Cu deposit, NW China: a case for increased depositional efficiency by reaction with mafic hostrock? Mineral. Deposita 1–23.
Shirey, S.B., Walker, R.J., 1995. Carius tube digestion for low-blank rhenium–osmium analysis. Anal. Chem. 67, 2136–2141.
Sillitoe, R.H., 1997. Characteristics and controls of the largest porphyry copper–gold and epithermal gold deposits in the circum-Pacific region. Aust. J. Earth Sci. 44, 373–388.
Sillitoe, R.H., 2010. Porphyry copper systems. Econ. Geol. 105, 3–41.
Sisson, T., Layne, G., 1993. H2O in basalt and basaltic andesite glass inclusions from four subduction-related volcanoes. Earth Planet. Sci. Lett. 117, 619–635.
Smith, C.M., Canil, D., Rowins, S.M., Friedman, R., 2012. Reduced granitic magmas in an arc setting: the Catface porphyry Cu–Mo deposit of the Paleogene Cascade Arc. Lithos 154, 361–373.
Sobolev, A.V., Chaussidon, M., 1996. H_2O concentrations in primary melts from supra-subduction zones and mid-ocean ridges: implications for H_2O storage and recycling in the mantle. Earth Planet. Sci. Lett. 137, 45–55.
Song, B., Li, J., Li, W., Wang, K., Wang, Y., 2002. SHRIMP dating of zircon from Dananhu and Keziekalasai granitoid batholith in southern margin of Tuiha basin, East Tishan, NW China and their geological implication. Xinjiang Geol. 20, 342–345.
Stein, H.J., Morgan, J.W., Scherstén, A., 2000. Re–Os dating of low-level highly radiogenic (LLHR) sulfides: the Harnäs gold deposit, Southwest Sweden, records continental-scale tectonic events. Econ. Geol. 95, 1657–1671.
Sun, S.S., McDonough, W.F., 1989. Chemical and Isotopic Systematics of Oceanic Basalts: Implications for Mantle Composition and Processes. In: Saunders, A.D., Norry, M.S.

(Eds.), Magmatism in the Ocean Basins. Geological Society of London, Special Publication.
Sun, Y., Sun, M., 2005. Nickel sulfide fire assay improved for pre-concentration of platinum group elements in geological samples: a practical means of ultra-trace analysis combined with inductively coupled plasma-mass spectrometry. Analyst 130, 664–669.
Sun, Y., Guan, X., Du, A., 1998. Determination of platinum group elements by inductively coupled plasma-mass spectrometry combined with nickel sulfide fire assay and tellurium coprecipitation. Spectrochim. Acta B 53, 1463–1467.
Sun, W., Zhang, H., Ling, M.-X., Ding, X., Chung, S.-L., Zhou, J., Yang, X.-Y., Fan, W., 2010. The genetic association of adakites and Cu–Au ore deposits. Int. Geol. Rev. 53, 691–703.
Sun, W.-d., Liang, H.-y., Ling, M.-x., Zhan, M.-z., Ding, X., Zhang, H., Yang, X.-y., Li, Y.-l., Ireland, T.R., Wei, Q.-r., Fan, W.-m., 2013. The link between reduced porphyry copper deposits and oxidized magmas. Geochim. Cosmochim. Acta 103, 263–275.
Tarkian, M., Stribrny, B., 1999. Platinum-group elements in porphyry copper deposits: a reconnaissance study. Mineral. Petrol. 65, 161–183.
Torgov, V.G., Demidova, M.G., Korda, T.M., Kalish, N.K., Shulman, R.S., 1996. Extraction-atomic absorption spectrometric method for the determination of the platinum group elements and gold in copper–nickel ores using an autoclave sample decomposition technique. Analyst 121, 489–494.
Totland, M.M., Jarvis, I., Jarvis, K.E., 1995. Microwave digestion and alkali fusion procedures for the determination of the platinum-group elements and gold in geological materials by ICP-MS. Chem. Geol. 124, 21–36.
Ulrich, T., Gunther, D., Heinrich, C.A., 1999. Gold concentrations of magmatic brines and the metal budget of porphyry copper deposits. Nature 399, 676–679.
van Keken, P.E., Hacker, B.R., Syracuse, E.M., Abers, G.A., 2011. Subduction factory: 4. Depth-dependent flux of H_2O from subducting slabs worldwide. J. Geophys. Res. Solid Earth 116, B01401.
Wallace, P.J., 2005. Volatiles in subduction zone magmas: concentrations and fluxes based on melt inclusion and volcanic gas data. J. Volcanol. Geotherm. Res. 140, 217–240.
Wang, Q., Xu, J.F., Jian, P., Bao, Z.W., Zhao, Z.H., Li, C.F., Xiong, X.L., Ma, J.L., 2006. Petrogenesis of adakitic porphyries in an extensional tectonic setting, dexing, South China: implications for the genesis of porphyry copper mineralization. J. Petrol. 47, 119–144.
Wang, Q., Wyman, D.A., Xu, J.F., Zhao, Z.H., Jian, P., Zi, F., 2007. Partial melting of thickened or delaminated lower crust in the middle of Eastern China: implications for Cu–Au mineralization. J. Geol. 115, 149–161.
Wang, M.F., Gutzmer, J., Michalak, P.P., Guo, X.N., Xiao, F., Wang, W., Liu, K., 2014. PGE geochemistry of the Fengshan porphyry-skarn Cu–Mo deposit, Hubei Province, Eastern China. Ore Geol. Rev. 56, 1–12.
Windley, B.F., Allen, M.B., Zhang, C., Zhao, Z.Y., Wang, G.R., 1990. Paleozoic accretion and Cenozoic redeformation of the Chinese Tien-Shan-Range, central-Asia. Geology 18, 128–131.
Wood, S.A., Pan, P., Zhang, Y., Mucci, A., 1994. The solubility of Pt and Pd sulfides and Au in bisulfide solutions. Mineral. Deposita 29, 309–317.
Xia, L.-Q., Xia, Z.-C., Xu, X.-Y., Li, X.-M., Ma, Z.-P., 2008. Relative contributions of crust and mantle to the generation of the Tianshan Carboniferous rift-related basic lavas, northwestern China. J. Asian Earth Sci. 31, 357–378.
Zhang, L.C., Qin, K.Z., Ying, J.F., Xia, B., Shu, J.S., 2004. The relationship between ore-forming processes and adakitic rock in Tuwu–Yandong porphyry copper metallogenic belt, eastern Tianshan mountains. Acta Petrol. Sin. 20, 259–268.
Zhang, L., Xiao, W., Qin, K., Qu, W., Du, A., 2005. Re–Os isotopic dating of molybdenite and pyrite in the Baishan Mo–Re deposit, eastern Tianshan, NW China, and its geological significance. Mineral. Deposita 39, 960–969.
Zhang, L.C., Wan, B., Li, W.Q., Tang, H.F., 2006a. Geochemistry and tectonic setting of copper-bearing porphyries on the southern margin of Tuba basin, Xinjiang. Acta Petrol. Sin. 22, 225–235.
Zhang, L.C., Xiao, W.J., Qin, K.Z., Zhang, Q., 2006b. The adakite connection of the Tuwu–Yandong copper porphyry belt, eastern Tianshan, NW China: trace element and Sr–Nd–Pb isotope geochemistry. Mineral. Deposita 41, 188–200.
Zhang, L., Qin, K., Xiao, W., 2008. Multiple mineralization events in the eastern Tianshan district, NW China: isotopic geochronology and geological significance. J. Asian Earth Sci. 32, 236–246.
Zhang, D., Zhou, T., Yuan, F., Fan, Y., Liu, S., Peng, M., 2010. Geochemical characters, metallogenic chronology and geological significance of the Yanxi copper deposit in eastern Tianshan, Xinjiang. Acta Petrol. Sin. 3327–3338.
Zhang, D., Zhou, T., Yuan, F., Fan, Y., Deng, Y., Xu, C., Zhang, R., 2014. Genesis of Permian granites along the Kangguer Shear Zone, Jueluotage area, Northwest China: Geological and geochemical evidence. Lithos 198–199, 141–152.
Zheng, Y.-C., Hou, Z.-Q., Li, W., Liang, W., Huang, K.-X., Li, Q.-Y., Sun, Q.-Z., Fu, Q., Zhang, S., 2012. Petrogenesis and geological implications of the Oligocene Chongmuda-Mingze adakite-like intrusions and their mafic enclaves, southern Tibet. J. Geol. 120, 647–669.
Zhou, M.F., Lesher, C.M., Yang, Z.X., Li, J.W., Sun, M., 2004. Geochemistry and petrogenesis of 270 Ma Ni–Cu–(PGE) sulfide-bearing mafic intrusions in the Huangshan district, Eastern Xinjiang, Northwest China: implications for the tectonic evolution of the Central Asian orogenic belt. Chem. Geol. 209, 233–257.
Zhou, T., Yuan, F., Zhang, D., Fan, Y., Liu, S., Peng, M., Zhang, J., 2010. Geochronology, tectonic setting and mineralization of granitoids in Jueluotage area, eastern Tianshan, Xinjiang. Acta Petrol. Sin. 26, 478–502.
Zindler, A., Hart, S., 1986. Chemical geodynamics. Annu. Rev. Earth Planet. Sci. 14, 493–571.